EPOC technical report

Uncertainty model and its projection on the representative grid

December 2021

Contents

Nomenclature

Notational conventions

$\hat{\cdot}$ means that the quantity has been *generated* or *approximated* in opposition to measured or observed.

A, B, C, ... a random variable is denoted by an upper-case letter.

a, b, c, ... a value of a random variable A, B, C, ... is denoted by a lower-case letter.

$\boldsymbol{A}$, $\boldsymbol{B}$, $\boldsymbol{C}$, ... a random vector is denoted by a bold-face letter.

$\mathcal{A}$, $\mathcal{B}$, $\mathcal{C}$, ... a set is denoted by a calligraphic letter.

Forecast error modelling - renewable and load uncertainty

X, Y, Z a random variable (upper case letter) of realization ($\mathbb{R}^+$), forecast ($\mathbb{R}^+$) and forecast error ($\mathbb{R}^+$). If required, the superscript specifies the type of forecast error between energy sources (wind or solar) and load, *e.g.*, Z^{solar} or Z^{load}.

x, y, z a value of X, Y, Z respectively.

X_t, Y_t, Z_t a random variable of realization ($\mathbb{R}^+$), forecast ($\mathbb{R}^+$), and forecast error ($\mathbb{R}$) at time t.

x_t, y_t, z_t a value of X_t, Y_t, Z_t.

T number of time steps (typically, $T = 24$).

$\boldsymbol{X}$, $\boldsymbol{Y}$, $\boldsymbol{Z}$ a random vector of realizations ($\mathbb{R}^T$), forecasts ($\mathbb{R}^{+,T}$), and forecast errors ($\mathbb{R}^{+,T}$) at T time steps $(X_1, \dots, X_T)$.

$\boldsymbol{x}$, $\boldsymbol{y}$, $\boldsymbol{z}$ a vector of values of $\boldsymbol{X}$, $\boldsymbol{Y}$, $\boldsymbol{Z}$.

N number of samples.

$\mathcal{Z}$ a set $\{\boldsymbol{z}^i\}_{i=1}^N$ of N samples of forecast errors $\boldsymbol{z}$.

Spatio-temporal modelling

In what follows, for the sake of conciseness, notations will be given for forecast errors only but these are very similar for realizations and forecasts.

Δ a difference in time $[h]$.

$Z_{t+\Delta}$ a random variable of forecast error at time $t + \Delta$.

ℓ, ℓ_k, ℓ^{lat}, ℓ^{lon} a location (the subscript k is for location k) defined by its coordinates $\ell = (\ell^{lat}, \ell^{lon})$: its latitude ℓ^{lat} and its longitude ℓ^{lon}.

L the number of locations.

Z_ℓ^i, $Z_{t,\ell}^i$, $\boldsymbol{Z}_\ell^i$, $z_{t,\ell}$ $z_{t,\ell}^i$, $\boldsymbol{z}_\ell^i$ a quantity (a random variable, a random vector, a value, a value vector) at time t and/or for sample/day i *at location* ℓ.

$\mathcal{Z}_\ell$ a set $\{\boldsymbol{z}_\ell^i\}_{i=1}^N$ of N samples of forecast errors $\boldsymbol{z}$ for location ℓ.

$\boldsymbol{Z}_L$ the concatenation of forecast error random vectors $Z_{\ell_1}, \dots, Z_{\ell_L}$ of L locations.

$\mathcal{Z}_L$ the concatenation of $\mathcal{Z}_{\ell_1}, \dots, \mathcal{Z}_{\ell_L}$ for the L locations.

R_{ℓ_k} a Voronoï cell of a location ℓ_k.

s_ℓ a load share (a fraction of the total load) associated to location ℓ.

α the decreasing exponential function parameter ($\mathbb{R}$).

d a distance [km].

$d(\ell_i, \ell_j)$ a function computing the Harvesine distance between locations ℓ_i and ℓ_j.

Scenario generation techniques

Cop a Gaussian copula.

u, $\boldsymbol{u}$ a value and a value vector drawn from respectively a univariate normal (Gaussian) distribution and a multivariate one, *i.e.*, $U \sim \mathcal{N}(0, \sigma)(= p_U)$ and $\boldsymbol{U} \sim \mathcal{N}(\mathbf{0}, \Sigma)(= p_{\boldsymbol{U}})$.

$\hat{z}$, $\hat{\boldsymbol{z}}$ a *generated* (*i.e.*, not measured) value and vector value of forecast error.

p_Z the probability density function (PDF) of Z.

$p_{\boldsymbol{Z}}$ the joint probability density function of $\boldsymbol{Z}$.

$\hat{p}_Z$, $\hat{p}_{\boldsymbol{Z}}$ the approximated PDF of Z and joint PDF of $\boldsymbol{Z}$.

F_Z the marginal cumulative density function (CDF) of Z, also referred to as the marginal of Z.

$F_{\boldsymbol{Z}}$ the joint cumulative density function of $\boldsymbol{Z} = (Z_1, \ldots, Z_T)$.

$\hat{F}_Z$, $\hat{F}_{\boldsymbol{Z}}$ the approximated CDF of Z and joint CDF of $\boldsymbol{Z}$.

Σ a covariance matrix.

Φ_Σ the cumulative density function of a multivariate Gaussian random variable with covariance matrix Σ.

ϕ, ϕ^{-1} the cumulative density function of a univariate Gaussian random variable, and its inverse.

φ, φ^{-1} a Normalizing Flow function, and its inverse.

θ the parameters of a Normalizing Flow.

φ_θ a Normalizing Flow with parameters θ.

J_φ a Jacobian matrix of partial derivatives of φ by $\boldsymbol{u}$. An element (i, j) of J_φ is the partial derivative of the i^{th} component of φ by the j^{th} component of $\boldsymbol{u}$, *i.e.*, $\frac{\partial \varphi_i}{\partial u_j}$.

C, c a random variable of a contextual information (a context), and a value of C.

$\boldsymbol{C}$, $\boldsymbol{c}$ a random vector of contextual random variables, and a value of $\boldsymbol{C}$.

Component uncertainty

A_t a binary random variable of availability at time t ($A_t = 0$ means that the component is unavailable at time t, and $A_t = 1$ means that the component is available at time t).

$\boldsymbol{A}$ a random vector $(A_1, \ldots, A_T)$ of availability $(\{0, 1\}^T)$.

λ the failure rate $[failures/year]$.

μ the repair rate $[repairs/year]$.

f the average failure frequency $[failures/year]$.

p_λ, p_μ, $\hat{p}_\lambda$, $\hat{p}_\mu$ probability of forced outage and recovery, and their approximated values.

$MTTR$ the mean time to repair $[h]$.

$MTTF$ the mean time to failure $[h]$.

1 Data sources

This section aims at presenting the different data sources in particular what they include and what has been derived (and how) from them.

1.1 RE-Europe

RE-Europe [Jensen and Pinson, 2017] is a synthetic dataset including:

- a transmission network model made of 1494 buses (24 in Belgium) and 2156 lines,
- weather-driven forecasts and realizations for wind and solar generations for a period of three years (hourly per bus),
- load realizations for a period of three years (hourly per bus).

All the buses of this network are associated to both wind and solar generation. A substation has only one bus, and each bus has only one node.

Load (demand) From the ENTSO-E transparency platform, Jensen and Pinson [2017] collect the data for the aggregated demand for each country hour per hour. In order to project these data at the required spatial resolution (of the network model), they split the country load signal proportionally to the population. Each bus of the network is associated to a load share (here proportionally to the population attached to this bus) in the total load. This procedure is referred in this document to as *load disaggregation*.

Renewable generation: Solar and wind Renewable power data are derived from ECMWF (weather forecasts) and COSMO-REA6 (weather realizations) data sets using reanalysis (details are given in the paper). Both data sets have a hourly temporal resolution and have spatial resolutions of respectively a grid of $16km \times 16km$ and $7km \times 7km$. ECWMF wind and solar forecasts are given every 12h (00:00 and 12:00) for the subsequent 90h. They also provide ECMWF *"realizations"* by stitching together most recent forecasts (*i.e.*, first 12h of each forecast).

In order to map these forecasts and realizations to network buses, Jensen and Pinson [2017] associate grid cells and network buses using a distance-based criterion: a bus and a grid cell are associated if

- the bus is closer to the grid cell than any other bus, or
- the grid cell is closer to the bus than any other grid cell.

It ensures that each bus receives data from at least one grid cell. Several grid cells may be associated to the same bus. Note that it may also be possible that a grid cell is associated to more than one bus, in this case, the contribution of the grid cell is split evenly among all associated buses (see paper for further details).

Additionally, similarly to load shares for load disaggregation, they provide two capacity layouts as a way of defining the fraction of the installed solar and wind capacities associated to each bus.

The uniform layout assigns to a bus a weight proportional to the area (sum of grid cells) associated to that bus. The proportional layout assigns to a bus a weight proportional to both the area associated to that bus and the bus' average capacity factor (*i.e.*, sum of yearly mean capacity factor of areas associated to that bus). Therefore, the proportional layout favors buses with high renewable potential, *i.e.*, with higher mean capacity factors. Both layouts can be used to split a country-aggregated installed capacity among network nodes.

1.2 TYNDP

TYNDP2020 includes a static grid that can be used as a representative grid of the future HV electrical network. It comes in a CGMES format and must be parsed in order to be usable. The CGMES format is described in the *dataset specification pdf* (`TYNDP 2020 ENTSO-E dataset specification.pdf`) in the TYNDP2020 folder. However, in a nutshell, the dataset is made of several files (EQ, TP, SSH and SV) and

each file is in the XML format that contains a set of classes (listed on page 9 of the *dataset specification pdf*). In the scope of the uncertainty model and its projection on the TYNDP grid, classes that refer to physical components of the network (*e.g.*, Substation, WindGeneratingUnit) are of interest. Functions to extract relevant information (*e.g.*, list of nuclear generating units) are provided where useful.

It should be noted that

(a) substations in TYNDP are not localized, *i.e.*without geographical coordinates,

(b) there is no historical data of renewable (wind or solar) generation realization or forecast,

(c) there are hourly time series of demand (load forecast) per country for different scenarios of the future generation and demand with different climate targets (by increasing renewable penetration, are named *National Trends*, *Global Ambition* and *Distributed Energy*) and for two or three years (in 2025, 2030 and 2040) depending on the scenario.

1.3 Elia

Elia shares on its website (elia.be) forecasts and realizations of load, solar and wind with various spatial resolutions. Load forecasts and realizations are only for the whole grid (country-level), solar-power generation forecasts and realizations are given per province, region (Wallonia, Flanders and Brussels) or country, and wind-power generation forecast are given per region (Wallonia, Flanders and Brussels) or country. Note that several forecasts are given such as week-ahead (D-7), day-head (D-1) and the *most recent forecast* (updated every hour). Note that missing most recent forecasts are replaced by the most recent *available* forecasts. Note also that these data are currently only used for illustrating this report.

1.4 ENTSO-E transparency platform

The ENTSO-E transparency platform (https://transparency.entsoe.eu) collects data about electricity generation, transportation and consumption data for the pan-European market. In the scope of the uncertainty model, we use the country-aggregated load forecasts and realizations. Note that the time resolution may vary across the different countries. For example, load data for Belgium are provided every 15 min, and every hour for France. Figure 1 illustrates the forecast error distribution of several countries during year 2020.

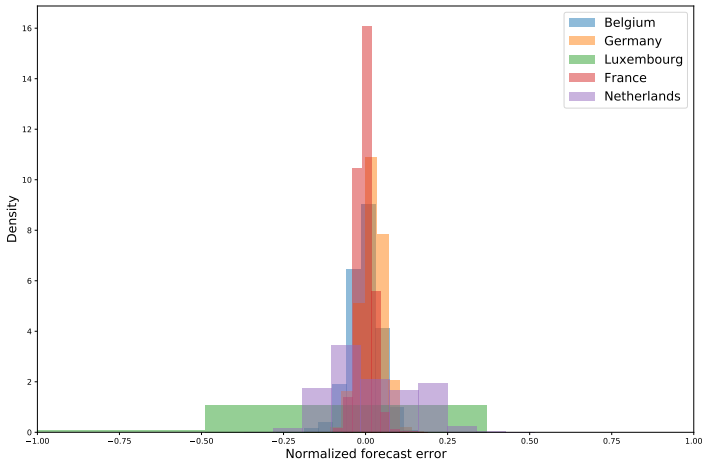

Figure 1: Forecast error distribution for several countries for year 2020 using ENTSO-E transparency platform data.

1.5 Others

PyPSA is an open-source network that approximates the European transmission network. The static grid has been derived using GridKit from the ENTSO-E interactive map by approximating location of every component of the network. It results in a static grid model with a localization of the substations.

2 Uncertainty model

This sections aims at explaining the modelling of the power injection uncertainty (wind, solar and load forecast errors) and component uncertainty. Note that this section is mostly theoretical while Section 3 describes how it is practically projected on the representative grid.

2.1 Uncertainty modelling

2.1.1 Power injection uncertainty

It can be used for either solar, wind or load.

Single location Let us model a realization of wind or solar generated power or load by a random vector $\boldsymbol{X} = (X_1, X_2, \ldots, X_T)$ where $X_t \in \mathbb{R}^+$ is the realization at time t and T is the number of time steps. To anticipate the future realization, forecasting tools are providing a forecast $\boldsymbol{Y} = (Y_1, Y_2, \ldots, Y_T)$ of $\boldsymbol{X}$ where $Y_t \in \mathbb{R}^+$. The actual realizations deviate from the forecast value, the difference $\boldsymbol{Z} = \boldsymbol{X} - \boldsymbol{Y}$ is the forecast error $\boldsymbol{Z} = (Z_1, \ldots, Z_T)$ where $X_t - Y_t = Z_t$ and $Z_t \in \mathbb{R}$. We may have past historical data of either realizations, or forecasts or both.

In this work, we have past values of realizations and forecasts from several data sources (see Section 1). Let us denote by x_t, y_t, z_t a value of X_t, Y_t, Z_t respectively, and by $\boldsymbol{x}$, $\boldsymbol{y}$, $\boldsymbol{z}$ a vector value of $\boldsymbol{X}$, $\boldsymbol{Y}$, $\boldsymbol{Z}$ respectively. Let us consider past historical data as a set of forecasts $\mathcal{Y} = \{\boldsymbol{y}^i\}_{i=1}^N$ and corresponding forecast errors $\mathcal{Z} = \{\boldsymbol{z}^i\}_{i=1}^N$, each made of N corresponding samples. In other words, sample $\boldsymbol{z}^i$ is the forecast error corresponding to the sample $\boldsymbol{y}^i$ (*i.e.*, $\boldsymbol{z}^i = \boldsymbol{x}^i - \boldsymbol{y}^i$ using a set $\mathcal{X} = \{\boldsymbol{x}^i\}_{i=1}^N$ of realization samples).

Here, we consider a hourly resolution, a day of measurements (*i.e.*, $T = 24$), and that every sequence of measurements starts at 00:00 and ends at 23:00. Thus, each sample corresponds to the measurements of a full day. Therefore, z_t^i corresponds to the forecast error at time t of sample/day i, and $\boldsymbol{z}^i$ is the sequence of forecast errors $(z_1^i, \ldots, z_T^i)$ at every time step of sample/day i.

Multiple locations This framework can be extended to model realizations, forecasts and forecast errors at several locations, where $X_{t,\ell}$, $Y_{t,\ell}$, $Z_{t,\ell}$ (resp., $x_{t,\ell}$, $y_{t,\ell}$, $z_{t,\ell}$) are respectively the realization, forecast, and forecast error for location ℓ at time t (resp. their value), and $\boldsymbol{X}_\ell$, $\boldsymbol{Y}_\ell$, $\boldsymbol{Z}_\ell$ (resp., $\boldsymbol{x}_\ell$, $\boldsymbol{y}_\ell$, $\boldsymbol{z}_\ell$) are respectively the random vectors of realizations, forecasts or forecast errors at location ℓ (resp., their value). Let us consider past historical data for L locations as two sets $\mathcal{Y}_L = \{\boldsymbol{y}_{\ell_1}^i, \ldots, \boldsymbol{y}_{\ell_L}^i\}$ and $\mathcal{Z}_L = \{\boldsymbol{z}_{\ell_1}^i, \ldots, \boldsymbol{z}_{\ell_L}^i\}_{i=1}^N$ which are the concatenations of sets $\mathcal{Y}_{\ell_1}, \ldots, \mathcal{Y}_{\ell_L}$ and sets $\mathcal{Z}_{\ell_1}, \ldots, \mathcal{Z}_{\ell_L}$ of the L locations $\ell_1, \ldots, \ell_L$.

The realizations, forecasts and forecast errors at several locations (simultaneous or not) may be spatio-temporally correlated. Spatial correlation will refer to correlation between realizations, forecasts and forecast errors that are simultaneous (*i.e.*, referring to the same time).

In this context, a scenario is a set of generated values for a day (*i.e.*, for each hour) for each location. We may therefore generate scenarios for either realizations, or forecasts or forecast errors. A scenario is therefore made of several random vectors (one for each location), that may be spatio-temporally correlated.

2.1.2 Component

Let us model the availability of a component throughout a day as a random vector of binary random variables $\boldsymbol{A} = (A_1, A_2, \ldots, A_T)$ where $A_t \in \{0, 1\}$ denotes the availability at time t (0 for unavailable and 1 for available). In our setting, we model the uncertainty of several components. Let us therefore

denote by $\boldsymbol{A}_k$ the availability random vector of component k, and by $A_{t,k}$ the availability of component k at time t.

2.2 Scenario generation techniques

A naive way of generating values from a distribution would be to assume that the error in predicting the random variable can be modelled as a Gaussian distribution centered around a predicted value. Intuitively, a Gaussian distribution is such that it is very likely to have a small value (around) zero meaning no or small forecast error (deviation from the forecast), and unlikely to have a large forecast error (large deviation from the forecast). Mathematically, we thus model the uncertainty as a Gaussian distributed random variable $\hat{x} = (1 + \epsilon)y$ where y is the forecast value, $\hat{x}$ is a generated realization[1], ϵ is a Gaussian random variable with zero mean if assuming that forecast errors are centered around the forecast value. However, by doing so, generated realizations are either uncorrelated if ϵ is different for every location and time step, or perfectly correlated if ϵ is the same for every location and time step. The following subsections present methods that are able to generate possible realizations that are (not perfectly) correlated with each other and therefore more realistic. Methods are first presented so as to generate forecast errors at a single location for a day (*i.e.*, generate values of $\boldsymbol{Z}$), then extended to generate forecast error at several locations. Generated values (in opposition to measured ones) are characterised by a hat on the symbol, *e.g.*, $\hat{z}$ is a generated forecast error value and $\hat{\boldsymbol{z}}$ is a generated vector value of forecast errors.

The Gaussian copula approach should be preferred in the end as it seems to be better known and used. However, the Normalizing Flows approach models scale differently with the number of locations and this may have an interest at some point.

2.2.1 Gaussian copula

Principle The idea of a Gaussian copula is to model *all* variables simultaneously by a multivariate Gaussian distribution that could generate values that are correlated with each other.

The Gaussian copula (GC) method models the dependence between forecast error variables by rewriting the joint cumulative density function $F_{\boldsymbol{Z}}$ (or, equivalently, $F_{Z_1,Z_2,\dots,Z_T}$) as follows

$$F_{\boldsymbol{Z}}(\boldsymbol{z}) = Cop(F_{Z_1}(z_1), \dots, F_{Z_T}(z_T)) \tag{1}$$

where F_{Z_t} is the CDF of variable Z_t corresponding to the forecast error at time t and Cop is a Gaussian copula Pinson et al. [2009], Golestaneh et al. [2016], *i.e.*,

$$C(F_{Z_1}(z_1), \dots, F_{Z_T}(z_T)) = \Phi_\Sigma(\phi^{-1}(F_{Z_1}(z_1)), \dots, \phi^{-1}(F_{Z_T}(z_T))) \tag{2}$$

where ϕ^{-1} is the inverse of the standard Gaussian CDF and Φ_Σ is the multivariate Gaussian distribution function with zero mean, unit marginal variance and a correlation matrix Σ.

In other words, the Gaussian copula approach models the interdependence of the forecast error variables $\boldsymbol{Z} = (Z_1, Z_2, \dots, Z_T)$ by the set of marginals $F_{Z_1}, F_{Z_2}, \dots, F_{Z_T}$ and a covariance matrix Σ of size $T \times T$.

Scenario generation Given a Gaussian Copula Cop with the set of marginals and the covariance matrix Σ, a scenario (*i.e.*, a generated value vector of forecast errors $\boldsymbol{z}$ and denoted by $\hat{\boldsymbol{z}}$) can be generated by first sampling T values from $\mathcal{N}(0, \Sigma)$ (denoted hereafter by $\boldsymbol{u} = (u_1, \dots, u_T)$) and then using Equation 2 (*i.e.*, applying Φ_Σ and then the corresponding inverse CDF to each component of $\boldsymbol{u}$). In the end, the generated $\{\hat{z}_t\}_{t=1}^T$ are correlated as characterised by the covariance matrix Σ.

Multiple locations The Gaussian copula framework can be extended to generate scenarios for several locations by considering simultaneously random vectors $\boldsymbol{Z}$ of different locations, *i.e.*,

$$\boldsymbol{Z}_L = (\boldsymbol{Z}_{\ell_1}, \boldsymbol{Z}_{\ell_2}, \dots, \boldsymbol{Z}_{\ell_p}) = (Z_{1,\ell_1}, \dots, Z_{T,\ell_1}, Z_{1,\ell_2}, \dots, Z_{T,\ell_2}, \dots, Z_{1,\ell_L}, \dots, Z_{T,\ell_L}) \tag{3}$$

where L is the number of locations and $\boldsymbol{Z}_{\ell_j}$ is the forecast error of location ℓ_j. Generate values for $\boldsymbol{Z}_L$ boils down to generating correlated values for $\boldsymbol{Z}$ of all locations.

[1] One can get a generated forecast error as follows $\hat{z} = \hat{x} - y$.

Contextual scenario generation In order to take into account some contextual information (*e.g.*, the average forecast, season, month, ...), one can simply build several Gaussian copula models, one per context. A context is defined by a set of values $\boldsymbol{c}$ of contextual variables[2] $\boldsymbol{C}$. For a given context $\boldsymbol{c}$, a contextual Gaussian copula can be built using only the past historical data in that context.

2.2.2 Normalizing Flows

Principle The Normalizing Flows (NF) principle is to estimate the probability density function $p_{\boldsymbol{Z}}(\boldsymbol{z})$ by learning a transformation $\varphi : \mathbb{R}^T \to \mathbb{R}$ mapping a multivariate Gaussian random variable[3] $\boldsymbol{u} \in \mathbb{R}^T$ and $\boldsymbol{z}$:

$$\boldsymbol{z} = \varphi(\boldsymbol{u}) \tag{4}$$

where φ is such that it is invertible and both φ and φ^{-1} are differentiable, $\boldsymbol{u} \sim p_{\boldsymbol{U}}(\boldsymbol{u})$ and $p_{\boldsymbol{U}}(\boldsymbol{u})$ is a known probability density distribution. In this context, the probability density of $\boldsymbol{Z}$ can be written as follows

$$p_{\boldsymbol{Z}}(\boldsymbol{z}) = p_{\boldsymbol{U}}(\boldsymbol{u}) |\det J_{\varphi}(\boldsymbol{u})|^{-1} \tag{5}$$

$$= p_{\boldsymbol{U}}(\varphi^{-1}(\boldsymbol{z})) |\det J_{\varphi^{-1}}(\boldsymbol{z})| \tag{6}$$

with $\boldsymbol{z} = \varphi(\boldsymbol{u})$ and thus $\boldsymbol{u} = \varphi^{-1}(\boldsymbol{z})$, and where $J_{\varphi}(\boldsymbol{u})$ is the Jacobian matrix of partial derivatives of φ by $\boldsymbol{u}$ (*i.e.*, element (i, j) of $J_{\varphi}(\boldsymbol{u})$ is $\frac{\partial \varphi_i}{\partial u_j}$).

In practice, $p_{\boldsymbol{U}}(\boldsymbol{u})$ is a multivariate normal and the transformation φ is built using a neural network φ_θ of parameters θ in order to provide an approximation $\hat{p}_{\boldsymbol{Z}}(\boldsymbol{z}; \theta)$ of $p_{\boldsymbol{Z}}(\boldsymbol{z})$. Parameters θ are trained from a set of samples $\mathcal{Z}$ by minimizing a loss, *e.g.*, by minimizing the Kullback-Leibler divergence between $p_{\boldsymbol{Z}}(\boldsymbol{z})$ and $\hat{p}_{\boldsymbol{Z}}(\boldsymbol{z}; \theta)$ (see more details, *e.g.*, in Papamakarios et al. [2019]). Many classes of NF exist but the autoregressive one is very popular because it makes the computation of the Jacobian determinant more tractable Huang et al. [2018], Papamakarios et al. [2017, 2019].

Scenario generation Once the mapping φ^{-1} from forecast errors ($\boldsymbol{Z}$) to a random variable ($\boldsymbol{U}$) of known distribution $p_{\boldsymbol{U}}(\boldsymbol{u})$ (*e.g.*, typically a normal distribution) is learnt, one can use the inverse transformation (φ is invertible by construction) to generate new scenarios by sampling from $p_{\boldsymbol{U}}$ and then applying φ_θ to derive scenarios $\hat{\boldsymbol{z}}$ (*i.e.*, a generated vector value of $\boldsymbol{z}$).

Multiple locations The location should be encoded as additional *contextual* variables (*e.g.*, with a one-hot encoding). Contextual variables $\boldsymbol{C}$ are variables that are used as inputs for the training the model **and** for generating values. That is, we have $\boldsymbol{u} = \varphi^{-1}(\boldsymbol{z}, \boldsymbol{c})$ (training) and $\boldsymbol{z} = \varphi(\boldsymbol{u}, \boldsymbol{c})$ (generation) where $\boldsymbol{c}$ are the values of $\boldsymbol{C}$.

2.2.3 Others

C-vine, D-vine, R-vine copulas follow the same principle as the Gaussian copula but instead of modeling all variables simultaneously (via a multivariate Gaussian random variable), these approaches use bivariate copulas (modelling variables two-by-two). These methods assume some dependence structures between variables in order to not model all pairs.

Instead of modeling the whole distribution, in these letter-vine approaches, some assumptions are made on the dependencies between variables. Therefore the joint distribution between $Z_1, \ldots, Z_T$ is decomposed as a product of simpler distributions and each of these simpler distributions is modelled by a copula.

2.3 Solar and wind forecast error scenario

Forecast errors are computed by taking the difference between realizations and corresponding forecasts. Figure 2 shows the distributions of wind and solar forecast errors using historical data of Wallonia during 4 years (2016 to 2019) from elia.be. It should be noted that probability distribution of forecast errors (Figure 2) show that they are centered around 0 (no error).

[2] To get a finite number of contexts, contextual variables should not be continuous but they should have a finite number of values. For example, forecast values can be discretized in forecast classes such as in Miettinen et al. [2020].

[3] In practice, it could be any multivariate random variable with a well-defined distribution.

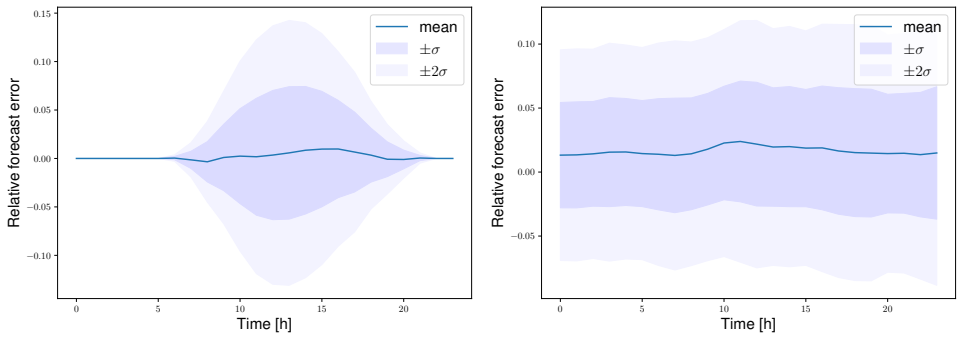

(a) PV (b) Wind

Figure 2: Forecast errors

It has been shown that wind and solar forecast errors are weakly correlated (but correlation increases with the size of the analyzed regions) [Zhang et al., 2013]. Therefore, they are modelled independently. In order to produce realization scenarios, they can be added on top of a reference forecast. Figures 3 and 4 show generated of PV and wind realizations respectively for two Belgian regions. Comparing the highlighted generated scenario (green solid lines) on left and right sides of each figure shows that it is similar (*e.g.*, more generation than anticipated) in both regions due to spatial correlation.

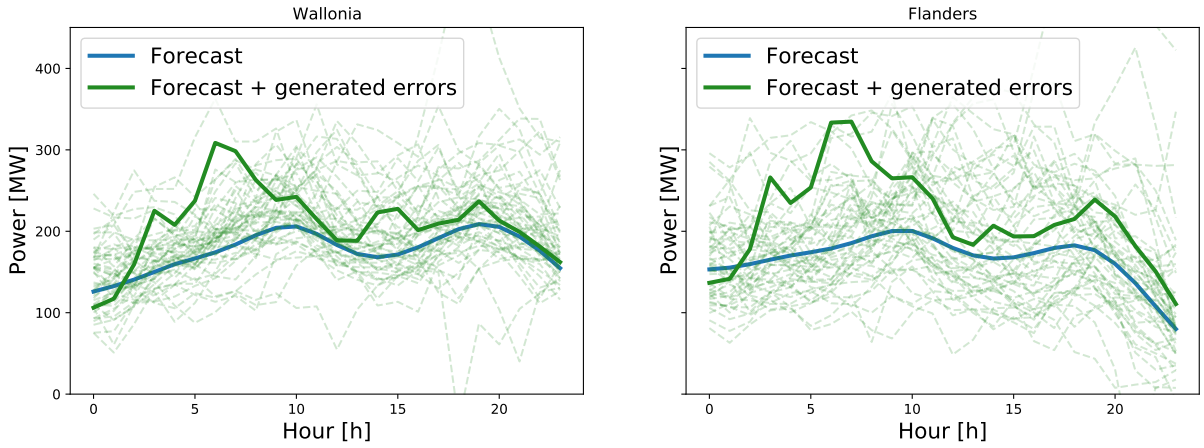

Figure 3: Generated realization scenarios for wind generation for two Belgian regions using the Gaussian copula approach using elia.be historical data.

As a reminder, we generate forecast errors scenario at a set of locations and an hourly resolution for a day ($T = 24h$).

2.4 Component uncertainty: forced outage and repair scenarios

This section aims at explaining how to generate scenarios of availability for a grid component[4].

2.4.1 Forced outage rates

The forced outage rate (unavailability) is given in Billinton and Allan [1992], Li [2014] as

$$U(FOR) = \frac{\lambda}{\lambda + \mu} = \frac{MTTR}{MTTF + MTTR} = \frac{f * MTTR}{8760} \tag{7}$$

where

[4]Currently, it is done for both generators and lines but this can be extended to transformers provided that data are available.

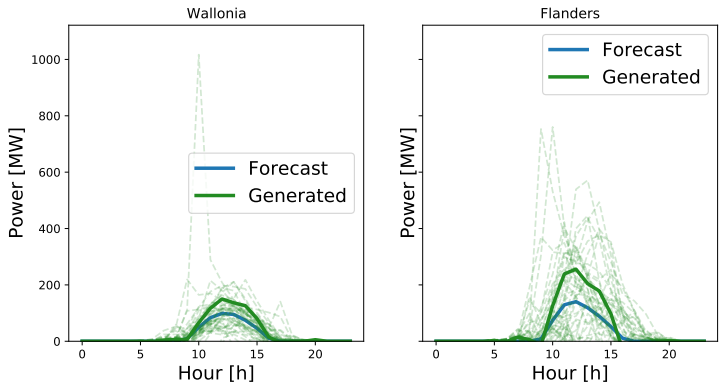

Figure 4: Generated realization scenarios for solar generation for two Belgian regions using the Gaussian copula approach using elia.be historical data. Note that generated stands for forecast + generated forecast errors.

- λ is the failure rate $[failures/year]$
- μ is the repair rate $[repairs/year]$
- $MTTR$ is the mean time to repair $[hours]$
- $MTTF$ is the mean time to failure $[hours]$
- f is the average failure frequency $[failures/year]$

Note that f and λ may be close in value but are two completely different quantities [Li, 2014].

2.4.2 Failure rate - probability of failure in [0,t]

For a static evaluation of the availability at some distant time in the future [Billinton and Allan, 1992, pg. 21] and in the case of generating equipment (*or component*) with relatively long operating cycles (not peaking or intermittent operating unit where multiple start-ups/shut-downs should be taken into account), the FOR is an adequate estimator of the probability that the unit under similar conditions will not be available for service in the future.

Probability of (no) forced outage within a short time period We assume the failure times to be exponentially distributed and only dependent on the component failure rates and not the maintenance times. Following Billinton and Allan [1992], the probability of experiencing exactly n failures in the period $[0, t]$ is

$$P(n) = \frac{(\lambda t)^n e^{-\lambda t}}{n!} \tag{8}$$

where n is the number of failure in time t, and λ is the (average) failure rate.

The probability of occurrence of a forced outage can be estimated using the Poisson distribution with a constant occurrence rate. That is, the probability of a forced outage not occurring within $[0, t]$ is given by

$$P(n = 0) = \frac{e^{-\lambda t}(\lambda t)^0}{0!} = e^{-\lambda t} \tag{9}$$

where λ is the average occurrence rate of a forced outage (*i.e.*, the failure rate), and t is the duration considered. The probability P_o of at least one forced outage occurring in $[0, t]$ is calculated by $1 - P(n = 0) = 1 - e^{-\lambda t}$. Consequently, the probability of failure in $t = 1[h]$ is $p_\lambda = 1 - \exp^{-\lambda_h}$ where λ_h is the failure rate per hour.

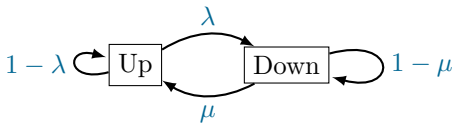

Figure 5: Two-state model

2.4.3 Repairable forced outage

Repairable forced outages are modelled by Billinton and Allan [1992] and Li [2014] as a two-state transition diagram (Figure 5).

Such a two-state model[5] corresponds to a cycle process alterning between up (available) and down (unavailable) states (Figure 6).

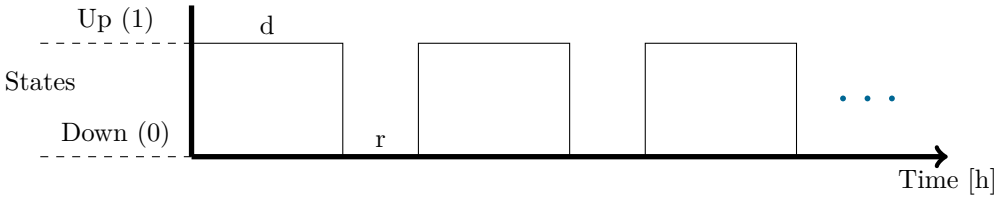

Figure 6: Two-state cycle process of a repairable component alternating up (available) and down (unavailable) states.

Similarly to the previous, the probability of recovery p_μ is calculated by $p_\mu = 1 - \exp^{-\mu_h}$ where μ_h is the repair rate per hour.

2.4.4 Generation of component availability scenarios

Scenarios of availability for each generator and line can be generated using a Monte-Carlo approach using the two-state model (Figure 6) following the pseudo-code described in Algorithm 1.

[5]Note that that probabilities λ and μ are unconditional (*i.e.*, do not depend on past events).

Data:

- Component probability of failure p_λ;
- Component probability of recovery p_μ;
- Component initial state (at time 0) $s_0 \in \{0, 1\}$.

Result: A vector $\boldsymbol{a} = (a_1, \ldots, a_T)$ (with $\boldsymbol{a} = \{0, 1\}^{24}$) where a_{t_i} gives the status of the component at time t_i, and the component is unavailable at time t_i if $a_{t_i} = 0$ and available if $a_{t_i} = 1$.

```
for each time step t_i = [1, 2, ..., 24] do
    Draw r_i ~ U[0,1] ;                                  /* Draw a random number.   */
    if a_{t_i - 1} = 0 ;                                 /* Component is unavailable. */
     then
        if r_i ≤ p_μ ;                                   /* Change state.   */
         then
            a_{t_i} = 1 ;                                /* Component becomes available.   */
        else
            a_{t_i} = 0 ;                                /* Component remains unavailable.   */
        end
    else
        if a_{t_i - 1} = 1 ;                             /* Component is available.   */
         then
            if r_i ≤ p_λ ;                               /* Change state.   */
             then
                a_{t_i} = 0 ;                            /* Component becomes unavailable.   */
            else
                a_{t_i} = 1 ;                            /* Component remains available.   */
            end
        end
    end
end
```

Algorithm 1: Generate a scenario of the availability of a component.

Scenario can be generated for every generator or line by using the appropriate probabilities of failure and recovery.

3 Projecting the uncertainty model on the representative grid

For the TYNDP grid, projecting the uncertainty model consists in

(a) generating forecast error scenarios for solar generation for all locations with solar generation,

(b) generating forecast error scenarios for wind generation for all locations with wind generation,

(c) generating forecast error scenarios for load for all locations,

(d) generating availability scenarios for every component (generators and lines).

3.1 Projection of the renewable uncertainty

In order to use the Gaussian copula approach for generating forecast error scenarios of wind and solar generation, we need to have marginals and a covariance matrix of pairwise spatio-temporal dependencies. Past measurements would have been sufficient but in the case of the TYNDP grid, there is no such historical data. Therefore, we propose to

- approximate the forecast error marginal distribution at a TYNDP substation by one derived from RE-Europe,
- estimate the spatio-temporal covariance matrix using a tree-based model.

To approximate the marginals, it mainly requires to

(a) localize TYNDP substations in order to associate them with RE-Europe ones with a distance-based criterion,

(b) associate each TYNDP substation with renewable generation with one from RE-Europe,

(c) compute the marginals of the RE-Europe and associate them to the corresponding TYNDP substations.

To build the spatio-temporal covariance matrix, it mainly requires to

(a) build a tree-based model that can predict spatio-temporal covariance between two locations using RE-Europe data,

(b) predict for each pair of location and time lag using the built model.

3.1.1 Localization of TYNDP substations

Information provided about the substations in the TYNDP varies accross the different countries. Table 1 shows the available information for each country. For Belgium, the following procedure has been followed:

(a) Find matches between TYNDP substations and PyPSA substations. Indeed, some PyPSA substations are described with their ENTSO-E label which corresponds in some case to the TYDNP substation names. As a reminder, PyPSA provides a list of substations with approximated coordinates from the ENTSO-E interactive map. While these coordinates are not exact, they are however sufficient to localize the substation in the right area.

(b) Automatic identification using an online map search-engine. Most substation names are derived from their location. As these may be street, town, city names, we may use the most likely result to localize the substation. However, let us note that several locations may have similar or identical names, and it may therefore be non trivial to do so.

(c) Manual identification using an online map search-engine. Similarly with the previous point, the substation name may be derived from a location name. However, these substations are sometimes abbreviated or slightly transformed in such a way to prevent an automatic match. A manual search helps to locate most of the remaining unlocalized substations. Note also that sometimes several substations have similar names that only differs from a number (*e.g.*, Tihange 1, Tihange 2, Tihange 3), these are assumed to be at the same location.

(d) Use links between substations to identify inconsistencies in steps (b) and (c). This step relies on two observations: (i) linked substations are likely to be rather close to each other and the line connecting them should have a reasonable length, (ii) unlocalized substations that are connected with localized substations may be easier to localize with that additional knowledge.

By applying these steps, most of the Belgian substations have been localized. Remaining substations are mostly generic names (*e.g.*, *BE_terminal*, *Tapping node line*, *dummy*). Figure 7 shows the Belgium map with every localized substations and it can be observed that locations appear to be consistent with respect to the lines between substations.

This procedure should be applied to other countries with either provided full substation name or abbreviation. Conversely, substations of countries with only numbers should be identified in a different way.

For the other CWE countries, some substations are only described by an abbreviation. In these case, we used static grids provided by TSOs (where main substations have their abbreviation and full name) to associate as much as possible abbreviations with their corresponding full names, before applying steps (a) to (d).

3.1.2 TYNDP substations with renewable generation

Not all substations are associated to renewable generation. Table 2 summarises the number of substations per country that are associated to either solar or wind generation. It should be noted that in some country (*e.g.*, Germany, Austria, Portugal) there is no substation associated to solar generation (solar generation is not explicitly labeled in TYNDP) while all countries have at least one substation associated to a wind generating unit.

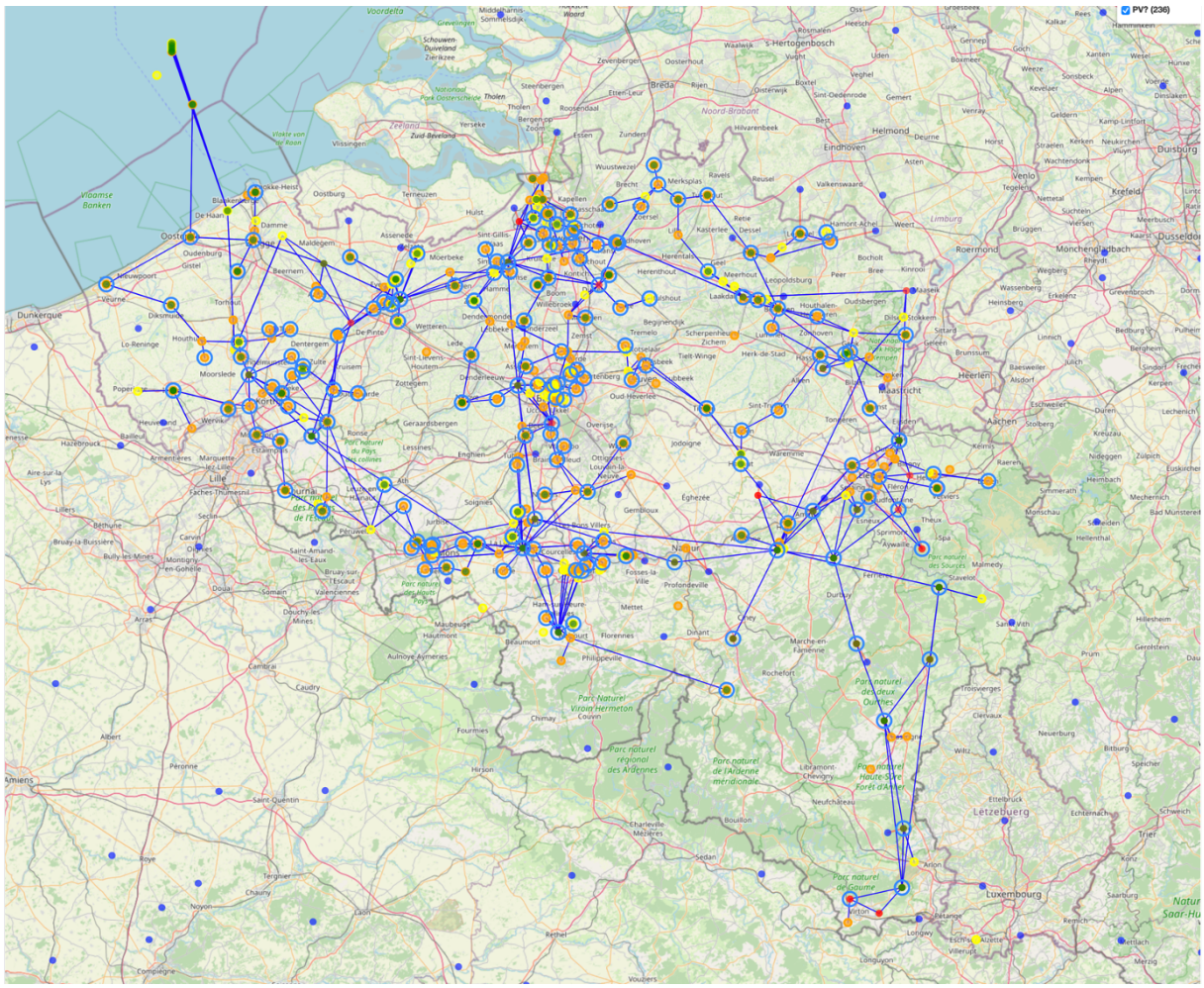

Figure 7: Localized TYNDP substations for Belgium and corresponding lines.

3.1.3 Association between RE-Europe and TYNDP

Each TYNDP substation is associated to the closest RE-Europe one using a distance-based criterion. From coordinates, it is possible to compute the distance using the Harvesine distance between two locations on a sphere:

The distance $d(\ell_x, \ell_y)$ is the Harvesine distance between two locations $\ell_x = (\ell_x^{lat}, \ell_x^{lon})$ and $\ell_y = (\ell_y^{lat}, \ell_y^{lon})$, where $\ell_x^{lat}, \ell_y^{lon}$ (resp. ℓ_y^{lat} and ℓ_y^{lon}) are respective the latitude and longitude of location ℓ_x (resp. ℓ_y), is equal to $d(\ell_x, \ell_y) = r \cdot c$ where

- $r = 6373.0$ [km],
- $c = 2\,\text{atan}_2(\sqrt{a}, \sqrt{1-a})$,
- $a = \sin^2\left(\frac{\ell_y^{lat} - \ell_x^{lat}}{2}\right) + \cos(\ell_x^{lat})\cos(\ell_y^{lat})\sin^2\left(\frac{\ell_y^{lon} - \ell_x^{lon}}{2}\right)$.

Similarly, we can divide Belgium into Voronoi cells using RE-Europe substations locations. A Voronoi cell is the area where every location within that cell is closer to the center of the cell than any other cell center. Mathematically, the Voronoi cell R_k centered around location ℓ_k is defined as

$$R_k = \{\ell_x | d(\ell_x, \ell_k) \leq d(\ell_x, \ell_j) \text{ for all } j \neq k\}.$$

Therefore, a TYNDP substation is associated to the center of the Voronoi cell it belongs. Figure 8 shows the results for Belgium using RE-Europe substations.

Country	Abb.	Name	ShortName	Description
Albania	AL	Abb.	✗	✗
Austria	AT	Full name	✗	✗
Belgium	BE	Abb.	✗	Full name (partially)
Bulgaria	BG	Full name	Number	✗
Switzerland	CH	Full name	✗	✗
Czech Republic	CZ	Abb.	Full name (partially)	✗
Germany	DE	Abb. or Full name	✗	✗
Denmark	DK	Abb.	✗	✗
Spain	ES	Number or Full name	✗	✗
France	FR	Abb.	✗	✗
Greece	GR	Abb.	✗	✗
Croatia	HR	Abb.	✗	✗
Hungary	HU	Abb.	✗	✗
Italy	IT	Abb. or Number	✗	✗
Luxembourg	LU	Abb.	✗	✗
Montenegro	ME	Number	✗	✗
North Macedonia	MK	Full name	✗	✗
Netherlands	NL	Number	✗	✗
Poland	PL	Abb.	idem 'Name'	Full name (partially)
Portugal	PT	Number	✗	✗
Romania	RO	Abb.	✗	✗
Serbia	RS	Number	✗	✗
Slovenia	SI	Full name	✗	✗
Slovakia	SK	Abb.	✗	✗

Table 1: Available information on substation in CGMES fields of IdentifiedObject *Name*, *ShortName* and *Description* per country. Bold face means main country of interest (Belgium), underlined means country of the CWE. Colors depict the difficulty to localize a substation (from green to red).

3.1.4 Computing forecast errors from RE-Europe

RE-Europe does not provide true past realizations and corresponding forecasts and is therefore not possible to compute the true past forecast errors. Therefore, they are several ways of deriving forecast errors from RE-Europe. One possiblity is to compute the difference between COSMO and ECWMF realizations[6]. Doing so, we would probably model the difference between two forecasting tools rather than the error of a single forecasting tool. Since ECMWF and COSMO may not be consistent with each other, this error may be larger than desired. Another possibility is to compute the forecast error at a given time step t by taking the difference of the realization (*i.e.*, the most recent forecast for t) and the forecast in day-ahead for time t (*i.e.*, the forecast made the previous day at 12:00). Figures 9 and 10 show the shapes of the forecast error distributions computed with both approaches.

3.2 Spatio-temporal correlation estimation

It has been observed in literature that there is a relationship between the spatial correlation of past measurements of wind and solar at two locations and the distance between these two locations. Typically, this relationship is modelled via a decreasing exponential of the form $e^{-\alpha.d}$ where d is the distance and α is a parameter adjusted on the data.

However, this dependency may vary over space and over time. Figures 11 and 12 shows that depending on the temporal difference, the point clouds (each point represents a pair (distance,correlation)) shifts from a decreasing exponential (no temporal difference, $\Delta = +0[h]$) to a straight constant line around 0. It is clear that a single model (*i.e.*, one single "curve") can not represent all points. Therefore there may be an interest of modelling this relationship with a more complex model (*i.e.*, more than one "curve"). In that end, we use a tree-based model to learn this relationship based on the following features for a pair

[6] As a reminder, ECWMF realizations are made by stitching together most recent forecasts.

Country	Abb.	Nb. substations	Nb. solar (TYNDP)	Nb. wind (TYNDP)
Albania	AL	269	2 (0.74%)	3 (1.12%)
Austria	AT	300	0 (0.00%)	49 (16.33%)
Belgium	BE	393	179 (45.55%)	113 (28.75%)
Bulgaria	BG	543	1 (0.18%)	11 (2.03%)
Switzerland	CH	130	71 (54.62%)	9 (6.92%)
Czech Republic	CZ	49	28 (57.14%)	17 (34.69%)
Germany	DE	691	0 (0.00%)	306 (44.28%)
Denmark	DK	175	76 (43.43%)	85 (48.57%)
Spain	ES	707	408 (57.71%)	343 (48.51%)
France	FR	1313	0 (0.00%)	490 (37.32%)
Greece	GR	2190	279 (12.74%)	250 (11.42%)
Croatia	HR	226	6 (2.65%)	21 (9.29%)
Hungary	HU	39	0 (0.00%)	9 (23.08%)
Italy	IT	698	274 (39.26%)	209 (29.94%)
Luxembourg	LU	38	5 (13.16%)	4 (10.53%)
Montenegro	ME	58	0 (0.00%)	3 (5.17%)
North Macedonia	MK	95	1 (1.05%)	2 (2.11%)
Netherlands	NL	615	0 (0.00%)	139 (22.60%)
Poland	PL	144	116 (89.56%)	97 (67.36%)
Portugal	PT	471	0 (0.00%)	52 (11.04%)
Romania	RO	94	21 (22.34%)	14 (14.89%)
Serbia	RS	428	0 (0.00%)	23 (5.37%)
Slovenia	SI	149	0 (0.00%)	1 (0.67%)
Slovakia	SK	27	16 (59.26%)	5 (18.52%)

Table 2: Number of substations, of substations associated to solar PV, of substation to wind generating units in TYNDP per country. Note that this table only summarises generating units that are described as solar PV in their description. Some countries (*e.g.*, France and Netherlands) specify PV or ZON in their generating unit names, while Germany considers solar PV generating as external network injections. This explains why some countries appear to not have solar PV generating units.

of locations (ℓ_x, ℓ_y):

1. Latitude of ℓ_x
2. Longitude of ℓ_x
3. Latitude of ℓ_y
4. Longitude of ℓ_y
5. Distance between ℓ_x and ℓ_y
6. Time (hour) at ℓ_x
7. Difference Δ (in hour) between time ℓ_y and time ℓ_x

Two approaches have been designed using either all features (spatio-temporal) or only spatial features (the first fifth ones, spatial). Figures 13 (spatial) and 14 (spatio-temporal) show the results for solar generated power and Figures 15 (spatial) and 16 (spatio-temporal) for wind generated power. These results clearly show that the spatio-temporal outperforms the temporal approach when there is a difference between times at x and at y. For wind, performances of both approaches are similar when there is no temporal difference ($\Delta = +0h$). This does not seem to be the case for solar but performances of the spatial approach are maximal when there is no temporal difference ($\Delta = +0h$).

3.2.1 Wind

Since wind generating unit is provided in TYNDP (see Table 2), wind forecast errors should only be generated for substations associated to wind generation.

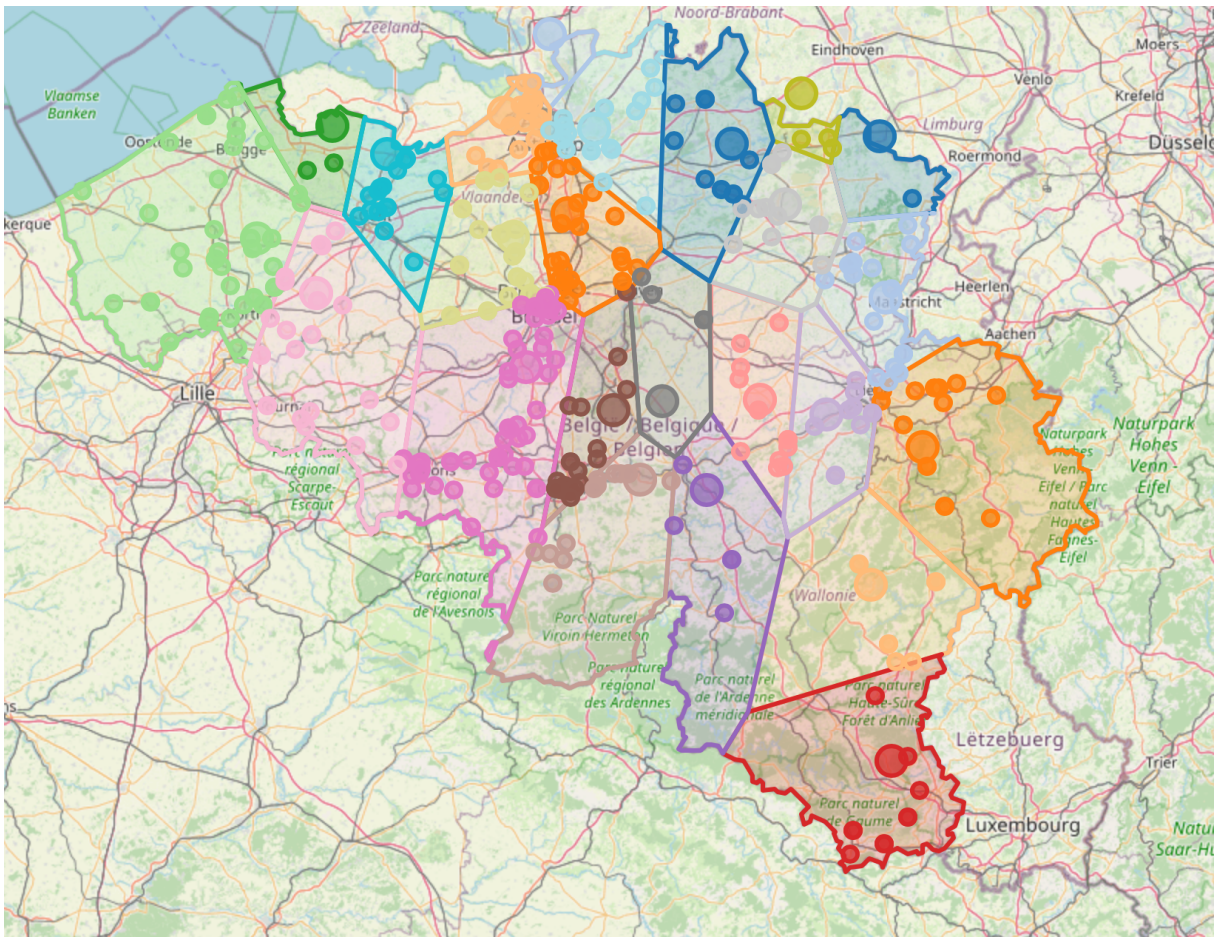

Figure 8: Voronoi cells using RE-Europe substation locations for Belgium. Bigger circles are for RE-Europe locations and center of Voronoi cells while small circles represent localized TYNDP substations and are colored according their associated RE-Europe substation.

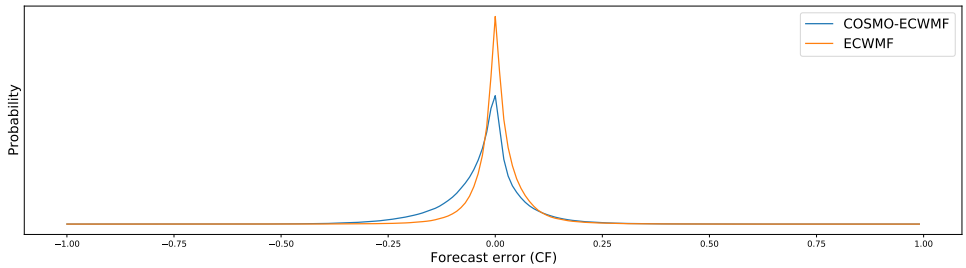

Figure 9: Difference of wind forecast error distributions when computing forecast errors from RE-Europe when using both COSMO and ECWMF, and only ECWMF.

3.2.2 Solar

Since solar generating units are not well reported in TYNDP (see Table 2), we assume that there is solar generation at every substation.

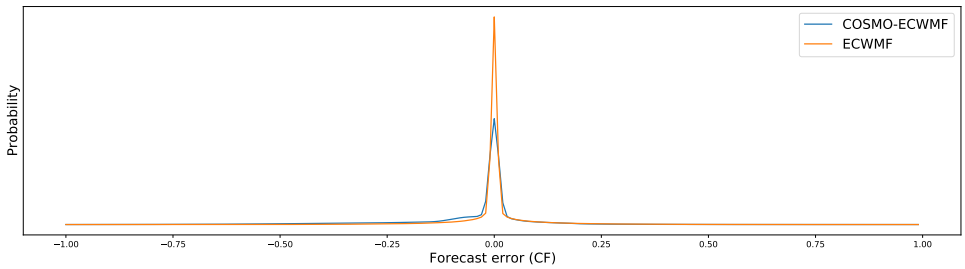

Figure 10: Difference of solar forecast error distributions when computing forecast errors from RE-Europe when using both COSMO and ECWMF, and only ECWMF.

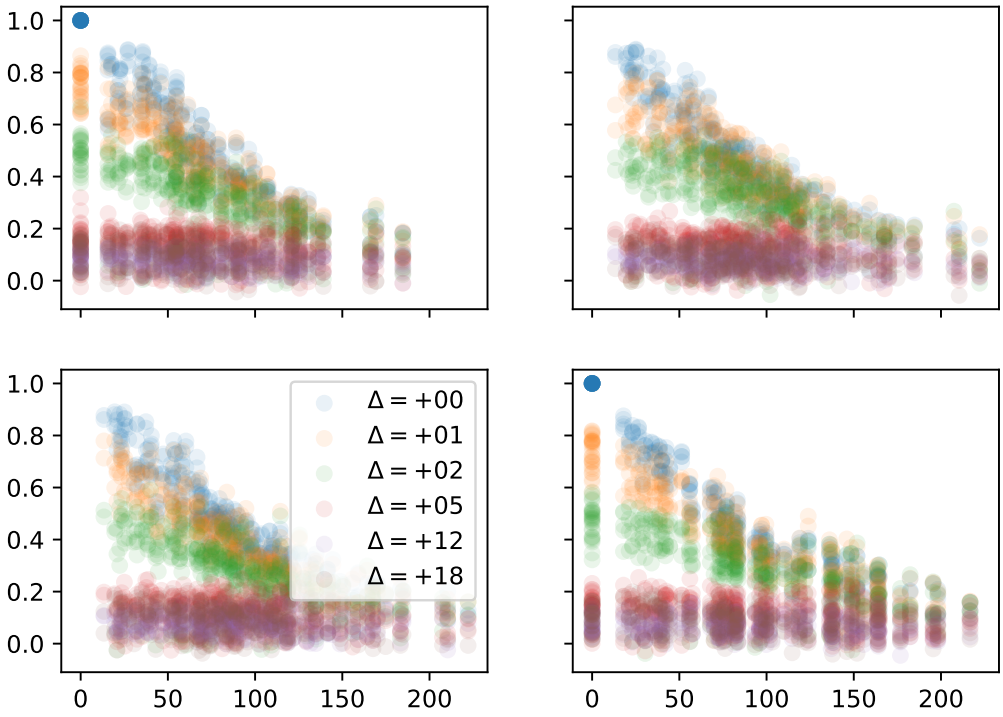

Figure 11: Point clouds for the relationship between distance (x-axis) and correlation (y-axis) between wind forecast errors of pairs of locations. Colors denote a temporal difference between considered measurements.

3.3 Projection of the load uncertainty

3.3.1 Load disaggregation

In TYNDP, ConformLoad are classes representing the load and are associated to substations. This can be used to derive the load share of each substation in the total load of a country: if l_i is the value associated to a substation i, then its load share $s_i = \frac{l_i}{\sum_j l_j}$ where the sum is over all substations.

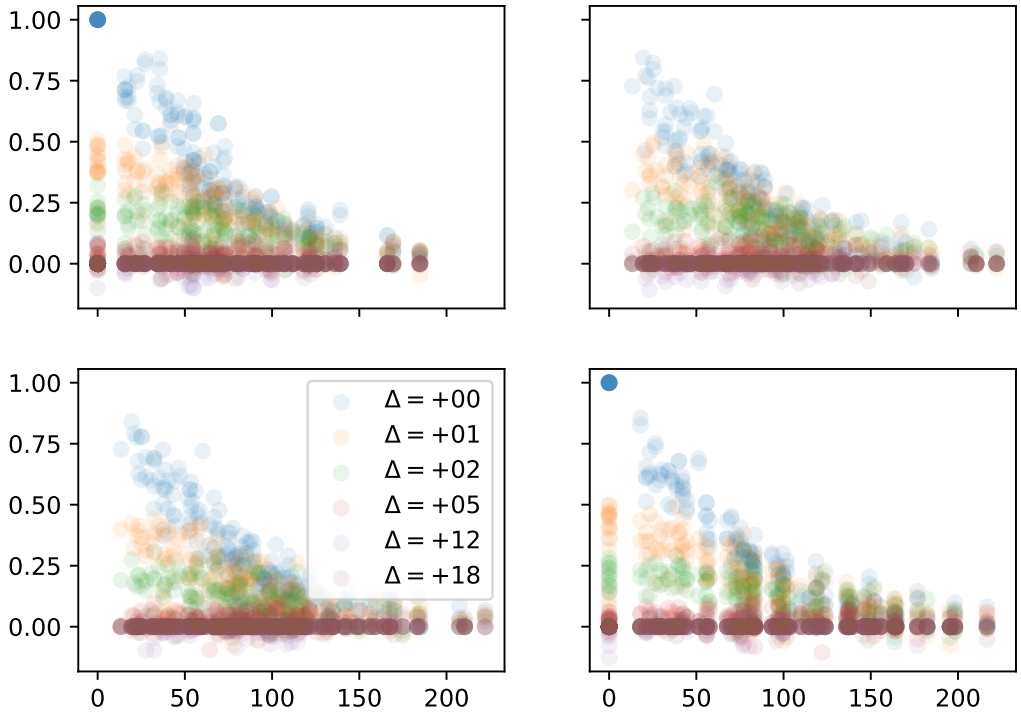

Figure 12: Point clouds for the relationship between distance (x-axis) and correlation (y-axis) between solar forecast errors of pairs of locations. Colors denote a temporal difference between considered measurements.

3.3.2 Load scenario generation

Forecast error scenario are generated using the Gaussian copula approach at the country level and then disaggregated using the substation load shares. This way of generating forecast error scenarios only models the spatio-temporal correlation *between countries*. Note that load shares used are derived from TYNDP and are always for the same for every time step.

3.4 Projection of the component uncertainty

Note that we did not search for data for transformers, however this could be considered for further extensions.

3.4.1 Forced outage rates of generators

From TYNDP, generators have been listed with their types and are grouped in four categories: *Nuclear*, *Thermal*, *Hydro* and *Others*. Depending on their types, generators are assigned to the corresponding forced outage and recovery probabilities. Probabilities are derived from several sources using formulas described in Section 2.4:

- elia.be: FOR, MTTF and MTTR are approximated from past forced outages.
- IEEE RTS (2019 update): FOR, MTTF [*h*], MTTR [*h*] are provided per component and we then average them by component type.
- Elia report (2019): FOR is provided by generator type (averaged over 2007-2017) with the MTTR [*h*] (averaged over 2007-2017).

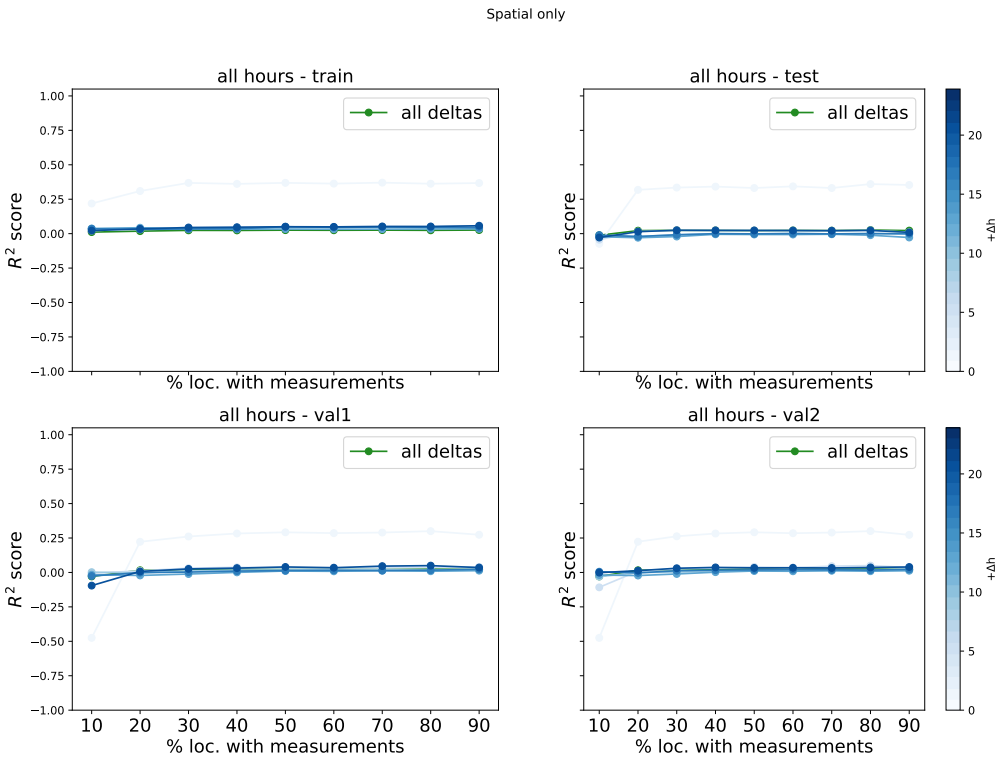

Figure 13: Evolution of the performance score (R^2 score) for the **spatial** approach with an increasing number of locations with **solar** measurements on the four data sets. Train is made of pairs of known locations, test is made of pair of unknown locations and val1 and val2 are for sets with only one known locations. Known locations are for locations with past measurements and unknown for those without. Color scale shows the temporal difference between locations. A blue curve corresponds to a model learnt only on data with the same temporal difference. Green curve shows when data with all temporal difference are used simultaneously.

3.4.2 Forced outage rates of lines

Similarly, lines are extracted from TYNDP and assigned to probabilities derived from one of the sources described in Section 3.4.1.

3.5 Table of methods

See excel files for a description of the different methods and how to use them.

3.6 Evaluation

This section summarises the evaluation protocol (see evaluation protocol for more details) and presents the main results of the evaluation of four methods.

3.6.1 Visual checks

Two visual checks can be used to visually comparing the generated scenarios with respect to the observations that have been used for the generation.

Distribution of observations vs distribution of generated scenarios The first visual check aims at comparing the generated forecast error scenarios with the observed forecast errors. The "distribution" of the generated forecast error scenarios is represented (both by minimal and maximal values at each time steps and with the 10% and 90% quantiles at each time step) along with the forecast error observations.

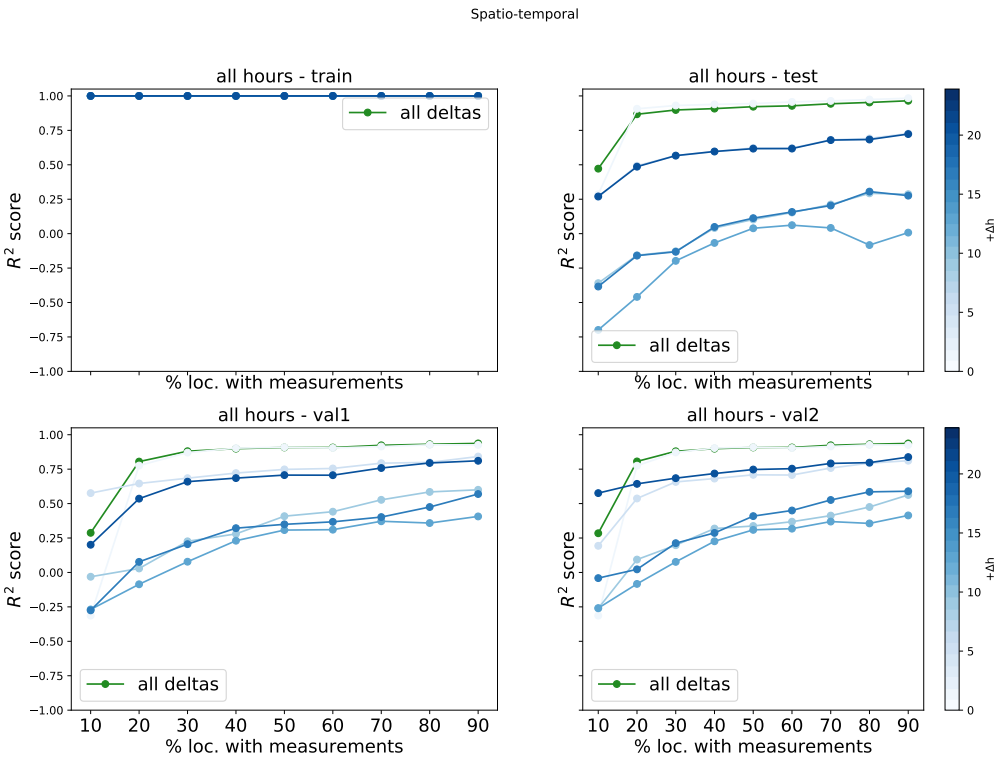

Figure 14: Evolution of the performance score (R^2 score) for the **spatio-temporal** approach with an increasing number of locations with **solar** measurements on the four data sets. Train is made of pairs of known locations, test is made of pair of unknown locations and val1 and val2 are for sets with only one known locations. Known locations are for locations with past measurements and unknown for those without. Color scale shows the temporal difference between locations. A blue curve corresponds to a model learnt only on data with the same temporal difference. Green curve shows when data with all temporal difference are used simultaneously.

The goal of such visual check is to show that generated forecast error scenarios appear to be realistic and similar to the observations.

Difference of forecast errors between close locations. The second visual check can be used to visually check whether the average absolute value of the difference of forecast errors between two (close) locations are similar to the observed average absolute value of the difference of forecast errors.

This visual check aims at showing whether the difference is well reproduced in the generated scenarios. If the curve for generated forecast error scenarios is similar to the one derived from the observations, it means that the difference of observed forecast errors between two close locations is well reproduced in the generated forecast error scenarios of close locations. This is a way of assessing visually the spatial correlation between forecast errors that we expect to be in the generated forecast error scenarios.

Note that the term "aligned" means that the difference in absolute value is computed between forecasts of two locations for the same scenario (in other words, if one generate 100 scenarios, one have 100 vectors of forecast error differences). The absence of the term "aligned" means that the difference is computed between forecast errors of one location for scenario i with forecast errors of another location for all scenarios, over all scenarios i. In other words, the comparison is not made for each scenario but across scenarios.

3.6.2 Quality assessment

For quality assessment, we considered the multivariate continuous ranked probability (or energy score) and the continuous ranked probability score (CRPS).

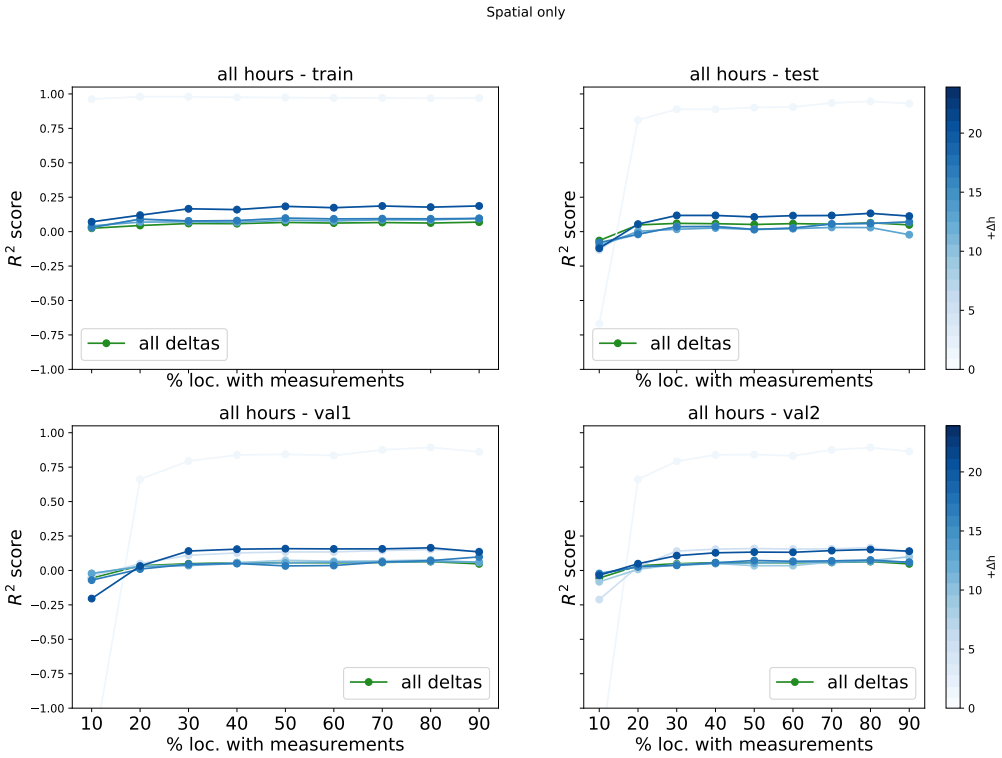

Figure 15: Evolution of the performance score (R^2 score) for the **spatial** approach with an increasing number of locations with **wind** measurements on the four data sets. Train is made of pairs of known locations, test is made of pair of unknown locations and val1 and val2 are for sets with only one known locations. Known locations are for locations with past measurements and unknown for those without. Color scale shows the temporal difference between locations. A blue curve corresponds to a model learnt only on data with the same temporal difference. Green curve shows when data with all temporal difference are used simultaneously.

The energy score assesses the quality of the generated forecast error scenarios. The CPRS is univariate and is compute for each time step. It therefore assesses the quality of the generated forecast error scenarios for a given time step.

Scenarios were generated for two months (January and June), with a fraction of the observations held out using the RE-Europe dataset.

3.6.3 Results for solar

Observations:

- June (Figure 18): all methods have very similar performances.
- January (Figure 17): Method 2 is less good than the three other methods. An explanation is that it generates scenarios that do not fit a typical solar power generation profile of January (e.g., less sun than in summer and longer night) because it does not take into account the temporal information while Method 9 and 5 do. Note also that Method 4 that also does not take into account the temporal information and is slightly less good at the beginning and the end of the bell curve.
- Visual checks of distributions (Figures 19 and 20): For both worst and best locations, distributions of generated forecast error scenarios seems to match the set of forecast error observations.
- Visual checks for differences (Figures 23 and 24): Unsurprisingly, normalizing flows methods (2 and 9) are not able to reproduce the difference of forecast errors for two close locations within the same scenario.

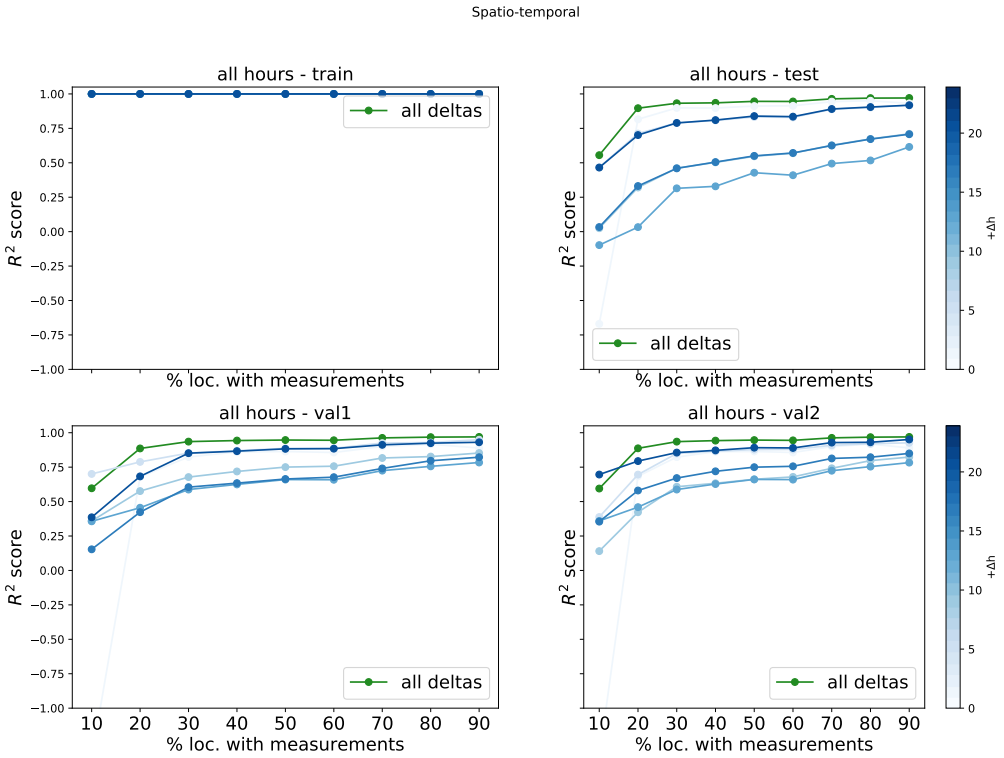

Figure 16: Evolution of the performance score (R^2 score) for the **spatio-temporal** approach with an increasing number of locations with **wind** measurements on the four data sets. Train is made of pairs of known locations, test is made of pair of unknown locations and val1 and val2 are for sets with only one known locations. Known locations are for locations with past measurements and unknown for those without. Color scale shows the temporal difference between locations. A blue curve corresponds to a model learnt only on data with the same temporal difference. Green curve shows when data with all temporal difference are used simultaneously.

3.6.4 Results for wind

Observations:

- Most observations are similar to solar forecast error scenarios evaluation.
- Gaussian copula methods tend to be slightly better however.
- Note that visual checks for distribution in January (especially for best location) show that Normalizing Flows methods can not capture "almost 0" forecast errors and therefore provide less good forecast error scenarios in that case.
- Similar observations can be drawn from the visual checks for difference of forecast errors.
- Note that CRPS per time step is higher at the end of the day because day-ahead forecasts should be less accurate for the end of the day than for the beginning (further in time), making forecast errors greater and probably forecast error scenarios also more difficult to generate for the end of the day.

3.6.5 Results for load

Results for load should be analyzed slightly differently. Load forecast error scenarios are generated at the aggregated level of the country, then disaggregated over the injections. Since the disaggregation scheme is static, forecast error scenarios of two close locations in the same country will be perfectly correlated

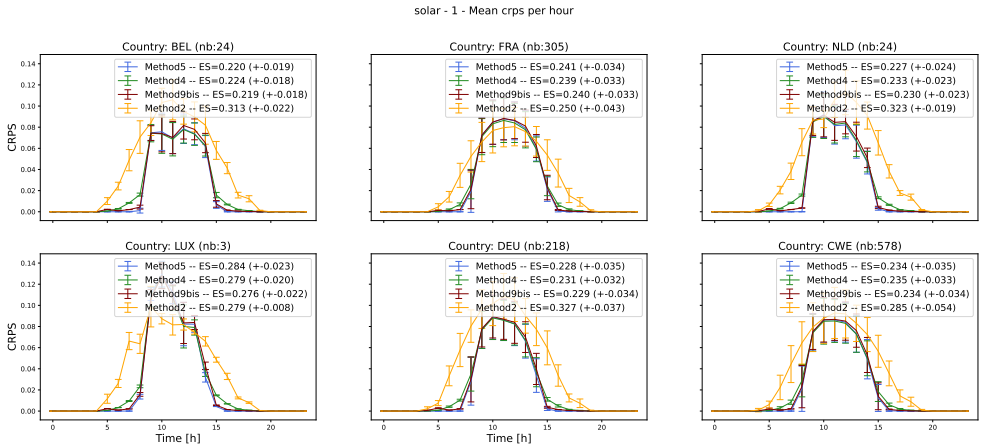

Figure 17: Results for solar in January.

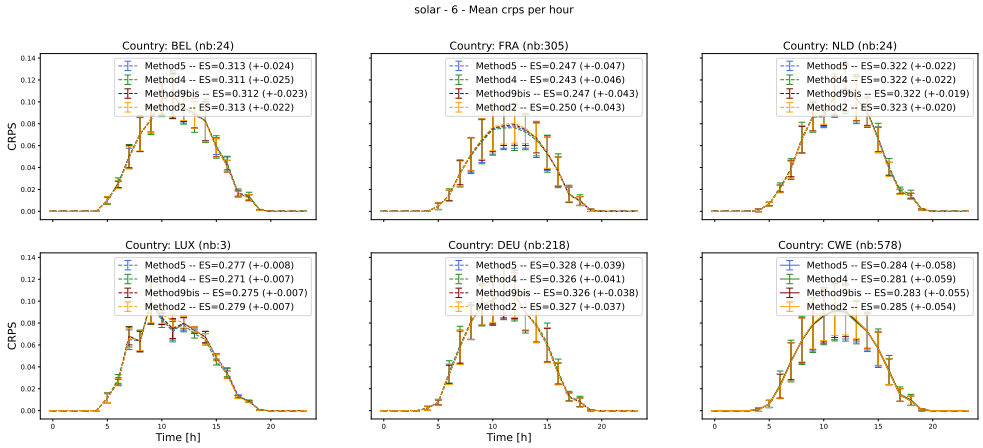

Figure 18: Results for solar in June.

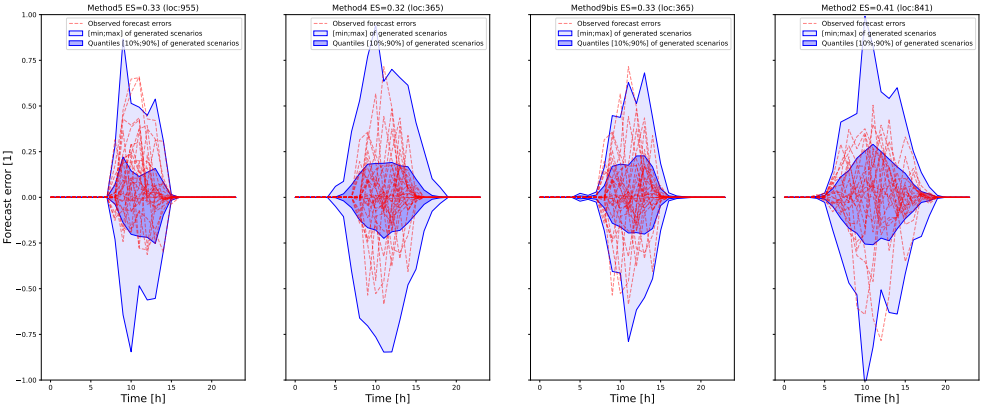

Figure 19: Visual check of distribution for solar in January (worst location).

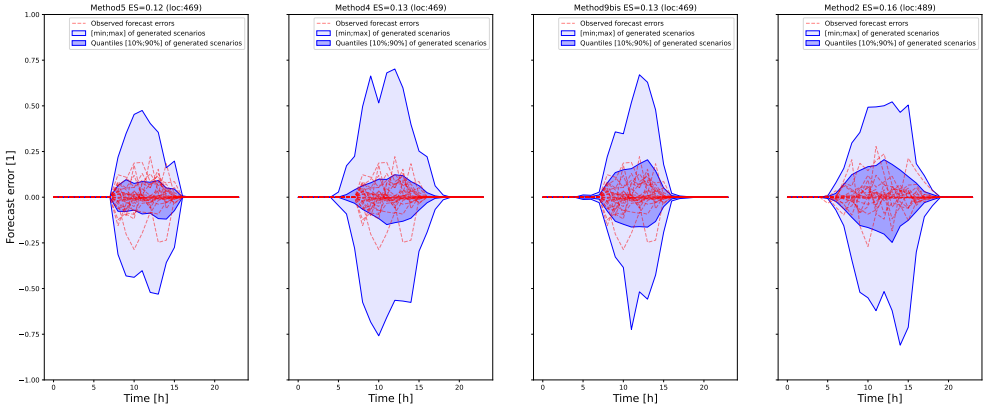

Figure 20: Visual check of distribution for solar in January (best location).

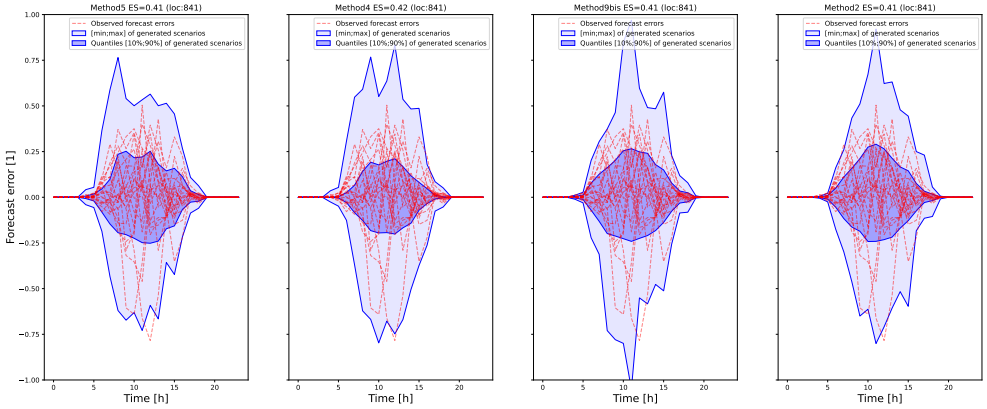

Figure 21: Visual check of distribution for solar in June (worst location).

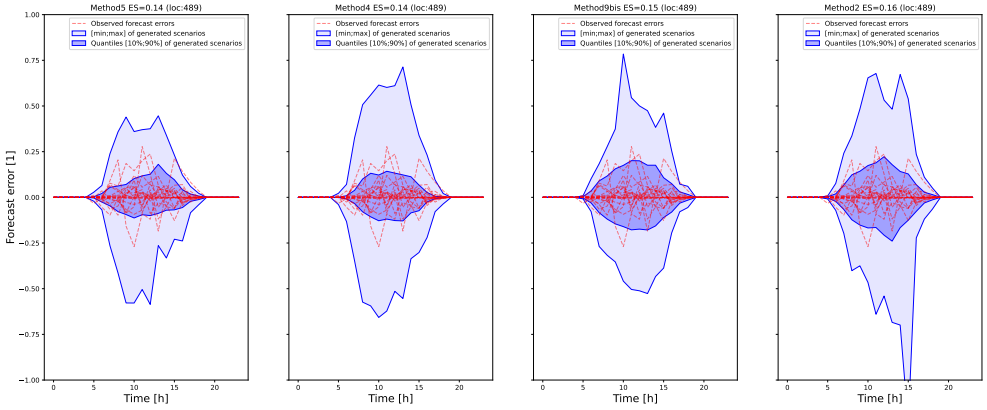

Figure 22: Visual check of distribution for solar in June (best location).

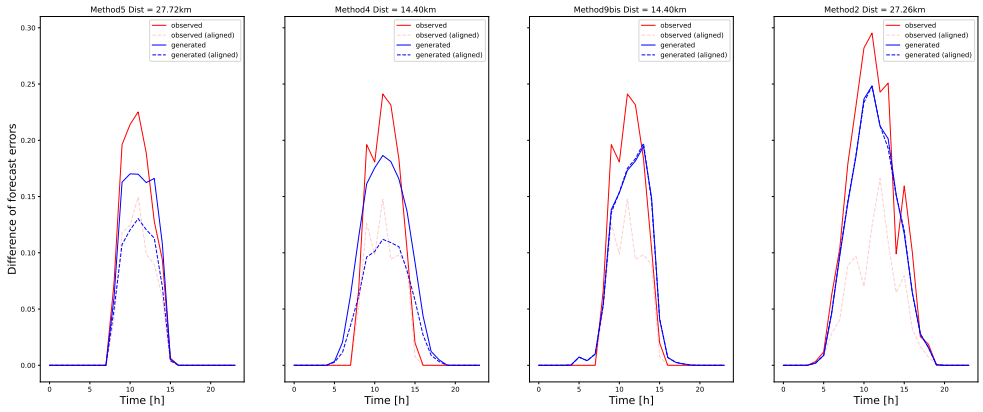

Figure 23: Visual check of differences for solar in January (worst location).

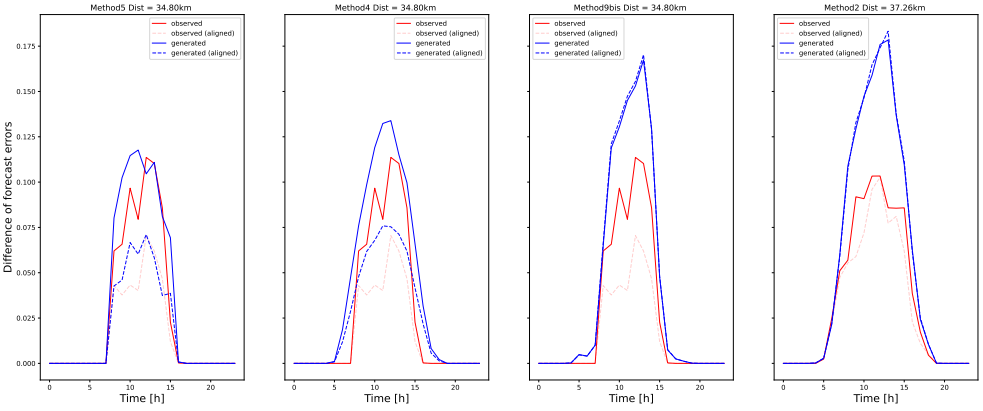

Figure 24: Visual check of differences for solar in January (best location).

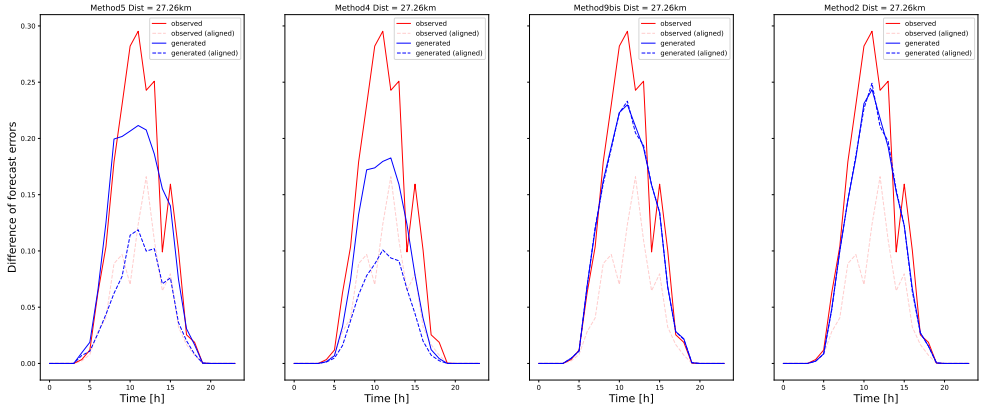

Figure 25: Visual check of differences for solar in January (worst location).

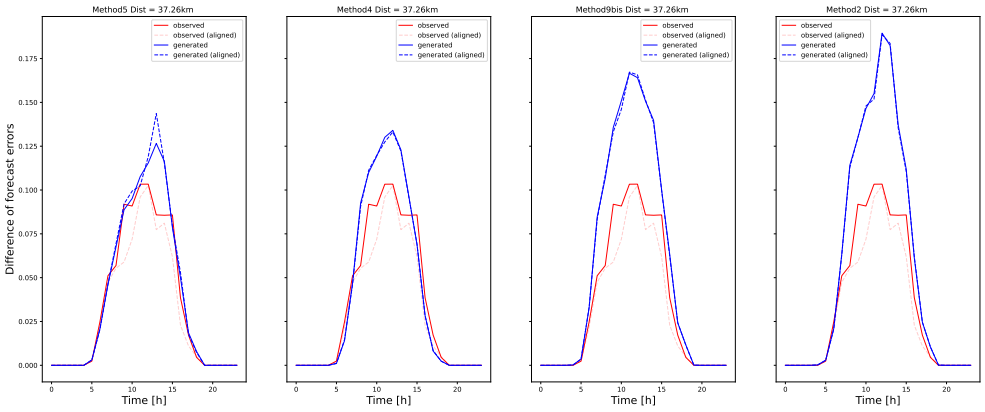

Figure 26: Visual check of differences for solar in January (best location).

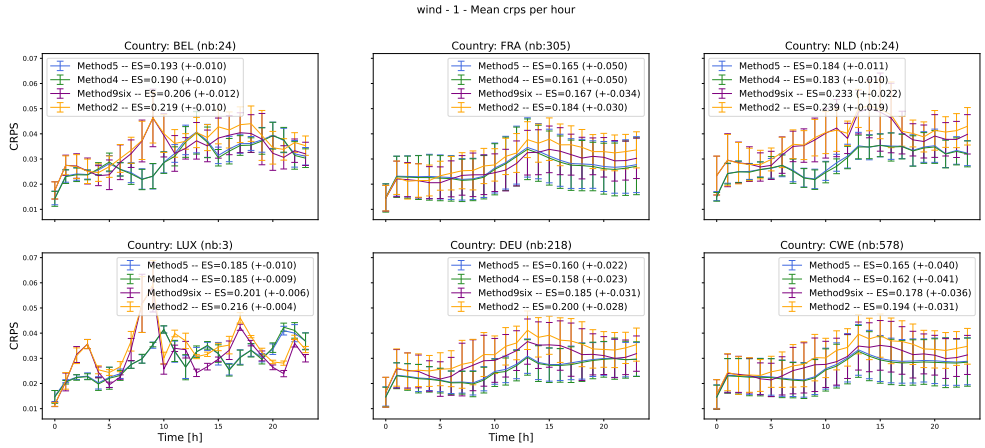

Figure 27: Results for wind in January.

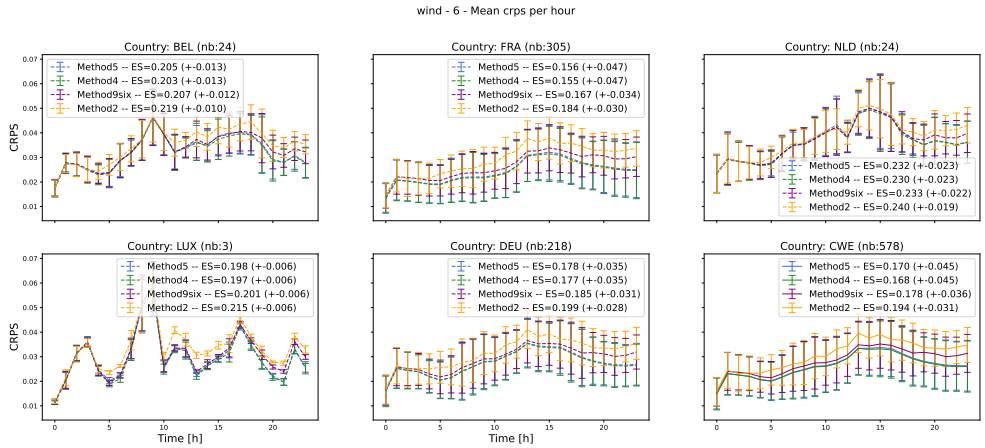

Figure 28: Results for wind in June.

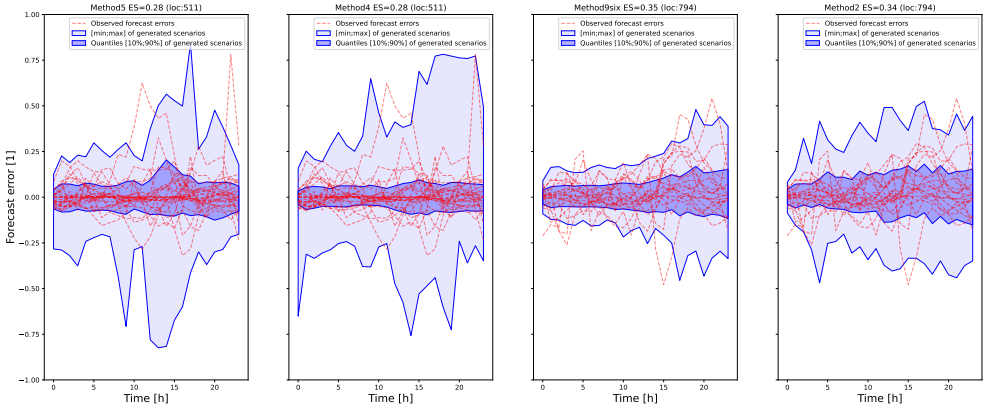

Figure 29: Visual check of distribution for wind in January (worst location).

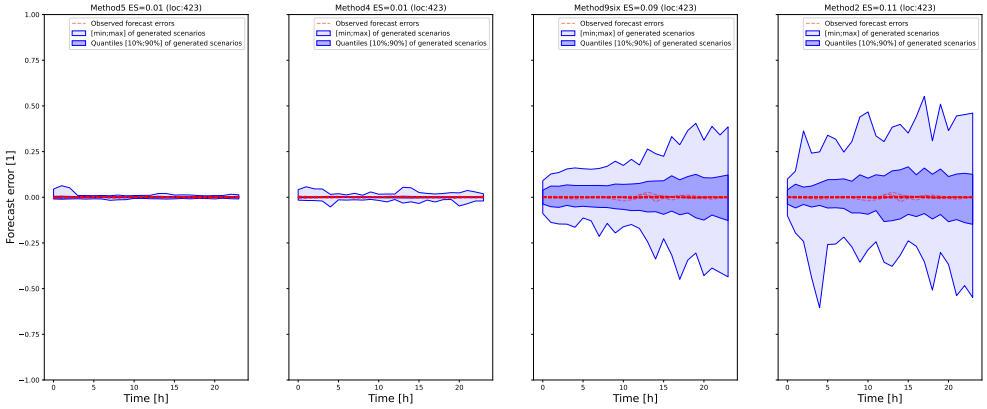

Figure 30: Visual check of distribution for wind in January (best location).

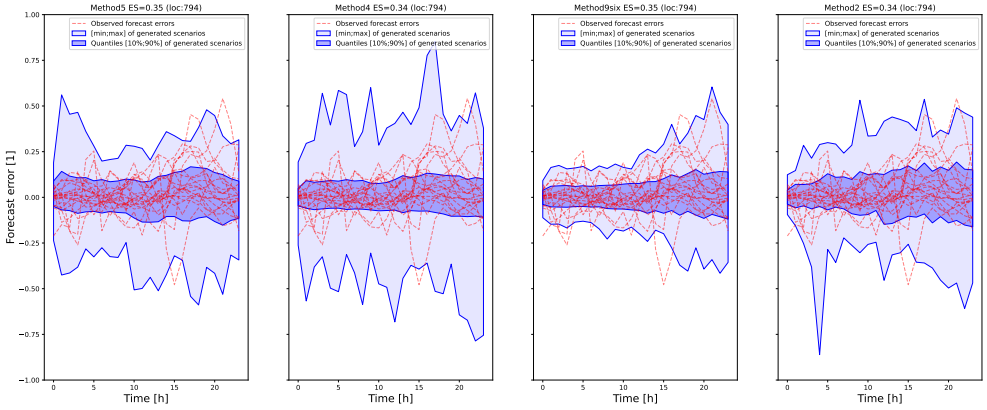

Figure 31: Visual check of distribution for wind in June (worst location).

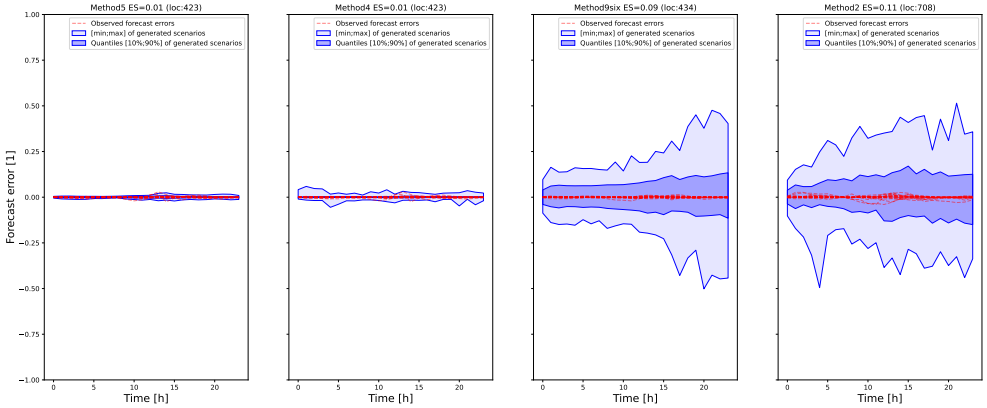

Figure 32: Visual check of distribution for wind in June (best location).

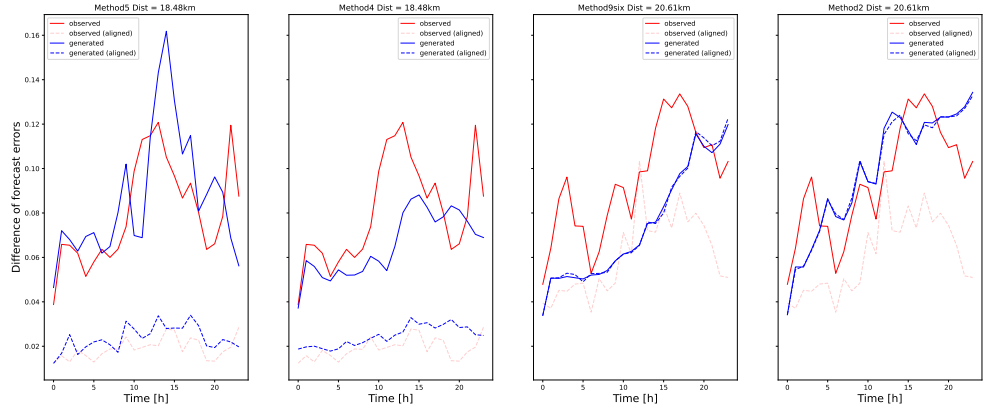

Figure 33: Visual check of differences for wind in January (worst location).

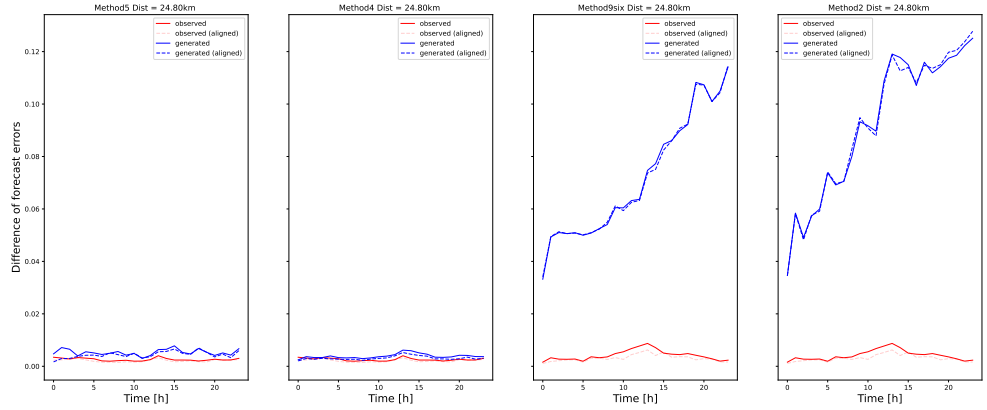

Figure 34: Visual check of differences for wind in January (best location).

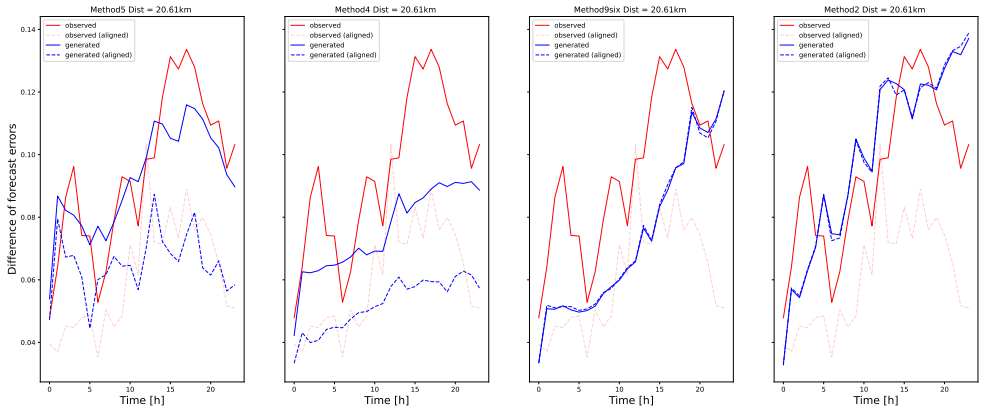

Figure 35: Visual check of differences for wind in January (worst location).

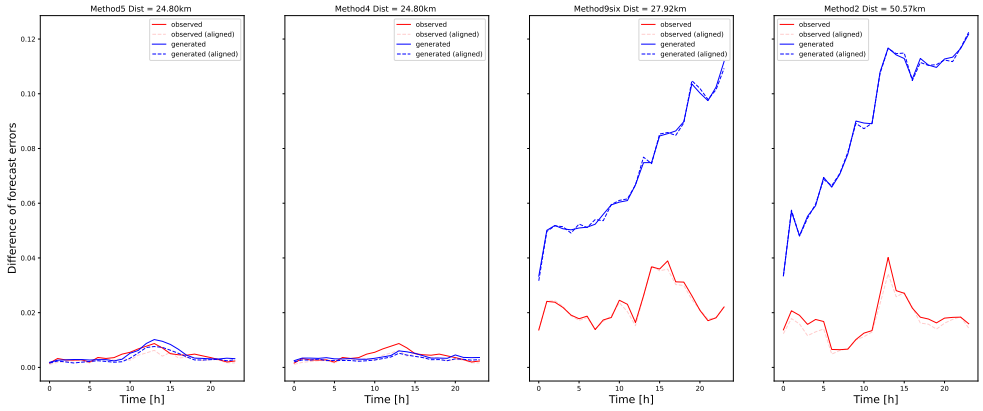

Figure 36: Visual check of differences for wind in January (best location).

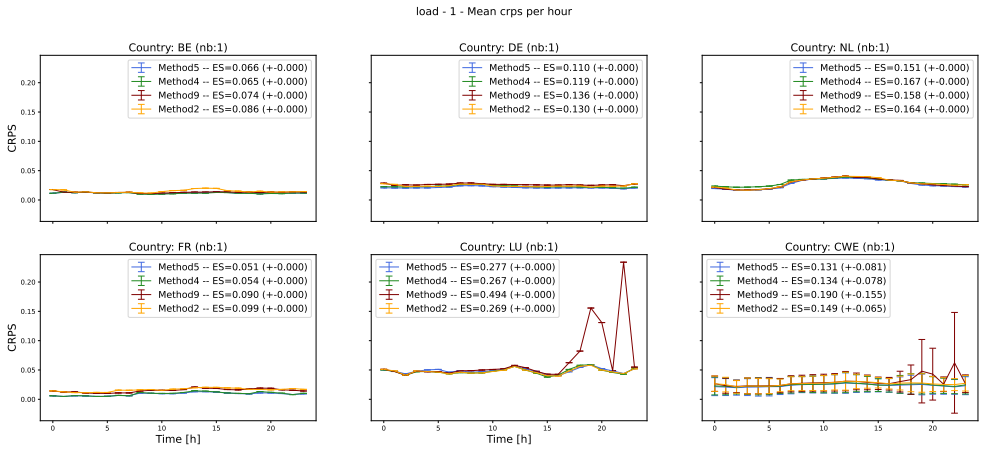

Figure 37: Results for load in January.

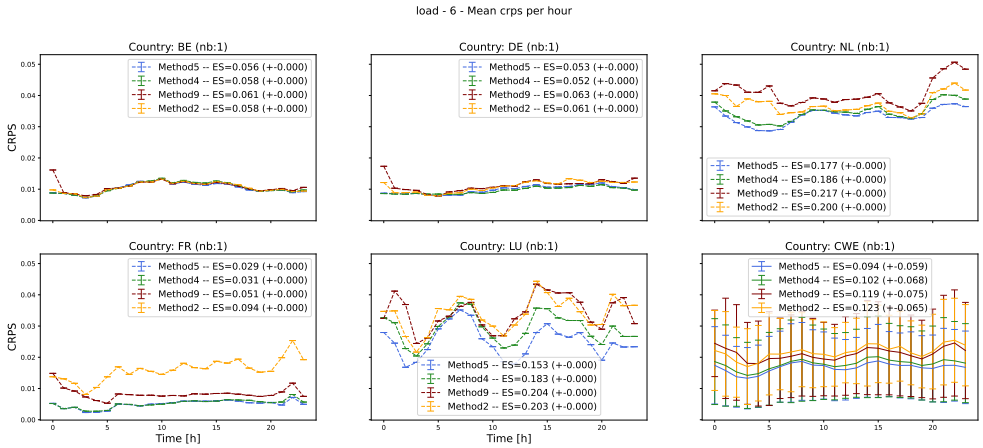

Figure 38: Results for load in June.

while they will be as correlated as the country forecast errors if the two close locations are in different countries. Note also that the model is much smaller, since only five countries are considered.

Figure 37 shows that methods are mostly similar over all countries except Luxembourg. Note that the aggregated-plot (bottom-right) is more impacted by the scores in Luxembourg (one fifth) than previously (3 injections over 578). Figure 38 (for June) shows that Normalizing Flows methods are slightly outperformed by Gaussian copulas methods.

Let's keep only the worst pair of locations. All Figures 39, 40, 41 and 42 show that, especially at the end of day, Normalizing Flows methods tend to generate very large values. Those large values have not been observed, resulting in less realistic generated forecast error scenarios. Overall, Gaussian Copulas seems to be more able to capture the correlation between the five countries.

Note that only one pair of locations is considered and is Belgium and Luxembourg as being the two closest locations.

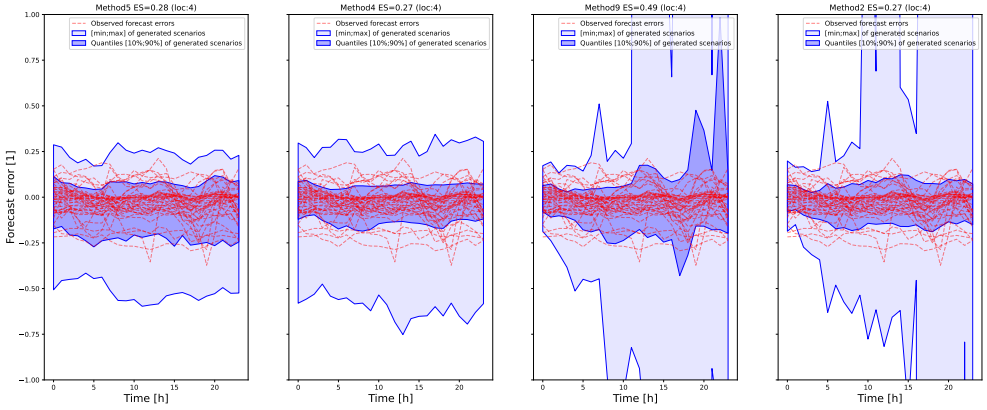

Figure 39: Visual check of distribution for load in January (worst location).

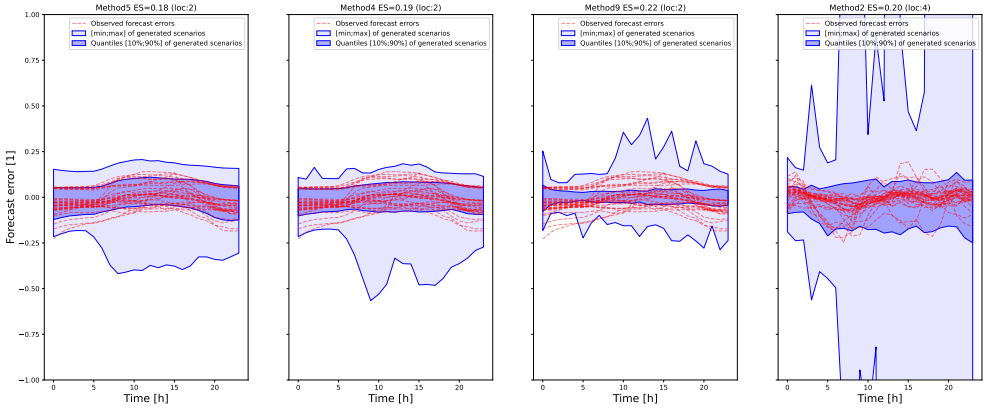

Figure 40: Visual check of distribution for load in June (worst location).

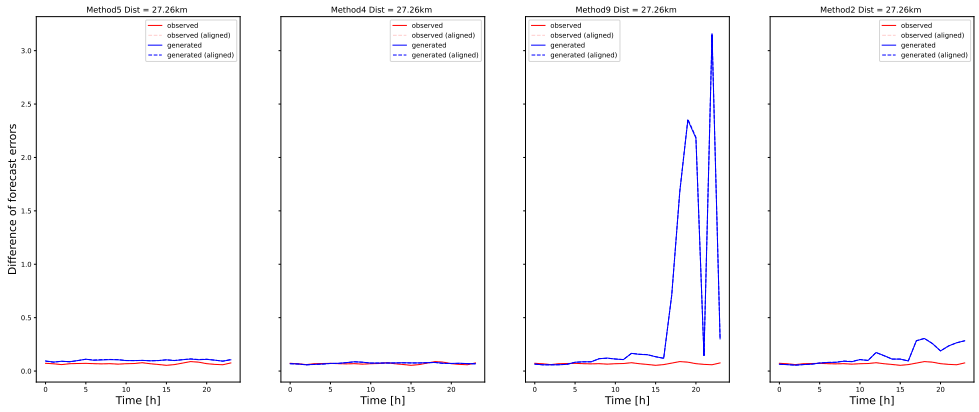

Figure 41: Visual check of differences for load in January (worst location).

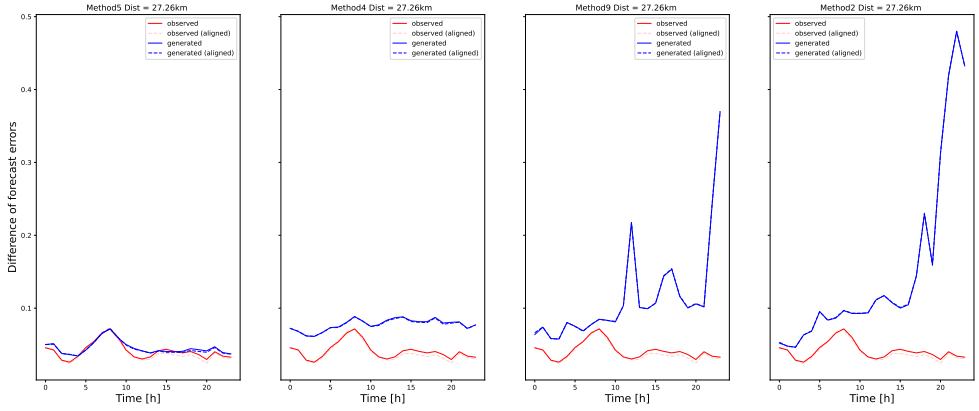

Figure 42: Visual check of differences for load in January (worst location).

References

Roy Billinton and Ronald Norman Allan. *Reliability evaluation of engineering systems*. Springer, 1992.

Faranak Golestaneh, Hoay Beng Gooi, and Pierre Pinson. Generation and evaluation of space–time trajectories of photovoltaic power. *Applied Energy*, 176:80–91, 2016.

Chin-Wei Huang, David Krueger, Alexandre Lacoste, and Aaron Courville. Neural autoregressive flows. In *International Conference on Machine Learning*, pages 2078–2087. PMLR, 2018.

Tue V Jensen and Pierre Pinson. Re-europe, a large-scale dataset for modeling a highly renewable european electricity system. *Scientific data*, 4(1):1–18, 2017.

Wenyuan Li. *Risk assessment of power systems: models, methods, and applications*. John Wiley & Sons, 2014.

Jari Miettinen, Hannele Holttinen, and Bri-Mathias Hodge. Simulating wind power forecast error distributions for spatially aggregated wind power plants. *Wind Energy*, 23(1):45–62, 2020.

George Papamakarios, Theo Pavlakou, and Iain Murray. Masked autoregressive flow for density estimation. *arXiv preprint arXiv:1705.07057*, 2017.

George Papamakarios, Eric Nalisnick, Danilo Jimenez Rezende, Shakir Mohamed, and Balaji Lakshminarayanan. Normalizing flows for probabilistic modeling and inference. *arXiv preprint arXiv:1912.02762*, 2019.

Pierre Pinson, Henrik Madsen, Henrik Aa Nielsen, George Papaefthymiou, and Bernd Klöckl. From probabilistic forecasts to statistical scenarios of short-term wind power production. *Wind Energy: An International Journal for Progress and Applications in Wind Power Conversion Technology*, 12(1): 51–62, 2009.

Jie Zhang, Bri-Mathias Hodge, and Anthony Florita. Investigating the correlation between wind and solar power forecast errors in the western interconnection. In *ASME 2013 7th International Conference on Energy Sustainability collocated with the ASME 2013 Heat Transfer Summer Conference and the ASME 2013 11th International Conference on Fuel Cell Science, Engineering and Technology*. American Society of Mechanical Engineers Digital Collection, 2013.